IGACtivities Newsletter
of the International Global Atmospheric Chemistry Project

Issue No. 21
September 2000

In this Issue

A Note From the IGAC Chair: *Guy Brasseur*

After the Aspen Meeting

Approximately 80 scientists representing the discipline of atmospheric chemistry and related sciences met in Aspen, Colorado from 28 April to 3 May 2000. The purpose of this large gathering was to review and improve a draft document (produced by a group of colleagues) summarizing our community's major scientific accomplishments of the last 10 to 20 years. Contributors were asked to synthesize progress within the framework of global change, and to identify questions remaining to be addressed.

The document produced as a result of this IGAC initiative is currently being finalized and in October will be evaluated by a group of about 50 anonymous reviewers. The resulting book should be published in mid-2001 by Springer-Verlag. When completed, this book, which represents an integrated view on several societally important questions, will be widely available not only within the scientific community, but also to decision makers in government and industry. It will provide the first international assessment of the state of knowledge on questions related to global tropospheric chemistry.

I would like to thank the different agencies, mostly in Europe, that are supporting this important IGAC initiative, as well as the lead and contributing authors, who have given a lot of their time to write and improve versions of the document.

This synthesis effort is part of an important transition for IGAC. Established some 12 years ago, IGAC has achieved many of its objectives and therefore needs to redefine its future directions and priorities. This task will begin in 2001. The new IGAC will likely address new issues over a spectrum of time scales, and be organized very differently from the present IGAC. Starting in early 2002, a new Chair will lead IGAC into its new era. The choice of the new Chair is an important task for both IGAC and its parent organizations, the CACGP and IGBP. The nomination process is open. Nominations should be communicated to Dr. Alex Pszenny (pszenny@mit.edu), the IGAC Core Project Officer, before December 1, 2000.

Tropospheric OH: In the beginning

Contributed by **Hiram Levy II** (hl@gfdl.gov), *Geophysical Fluid Dynamics Laboratory/NOAA, USA.*

Prior to 1971, most of the troposphere, with the exception of a few uniquely polluted regions, was thought to have a relatively benign photochemistry with the only exceptions being some possible ozone reactions. The oxidizing of trace gases, such as CO and CH_4, was thought to occur only in the stratosphere. For reviews from this period, see Bates and Witherspoon [1952], Junge [1963], and Cadle and Allen [1970]. Our theoretical understanding of the role of hydroxyl radicals (OH) in tropospheric chemistry evolved from earlier (1950s and 1960s) work in both the stratosphere and the polluted boundary layer.

Although an H_2O–O_3 chemical mechanism was developed in the 1950s for the mesosphere [e.g., Bates and Nicolet, 1950], it was not until the 1960s that Engleman [1965] identified the reaction that became essential to OH production in the troposphere:

$$O(^1D) + H_2O \rightarrow 2\ OH \qquad (R1)$$

This reaction and the earlier H_2O-O_3 reactions from the mesosphere were used to construct a H_2O-based catalytic destruction mechanism for stratospheric O_3 [Hampson, 1964; Hunt, 1966], but revised $O(^1D)$ quenching rates greatly reduced its stratospheric significance. The work of this period, which just precedes Crutzen's development of the NO_X catalytic destruction scheme [1970], is nicely summarized by Nicolet [1970].

At the same time that stratospheric research was identifying the key source of OH in the troposphere, studies of smog chemistry were beginning to focus on O_3 formation from hydrocarbon oxidation in polluted environments (for a detailed discussion of the early research, see P.A. Leighton, Photochemistry of Air Pollution, 1961). In the 1960s, smog chemistry research began to consider OH. Westberg and Cohen [1969] and Heicklen, Westberg and Cohen [1971] then proposed a catalytic mechanism to explain the O_3 formation observed in smog chambers, which would also provide an important component of the photochemical mechanism for the troposphere as a whole.

$$OH + CO + O_2 \rightarrow HO_2 + CO_2 \qquad (R2)$$

or

$$OH + RH \rightarrow RO_2 + H_2O \qquad (R3)$$

followed by

$$HO_2 + NO \rightarrow OH + NO_2 \qquad (R4)$$

or

$$RO_2 + NO \rightarrow RO + NO_2 \qquad (R5)$$

However, the rate coefficients for R4 and R5, which were the key, had not yet been measured. While estimates ranged from 1×10^{-11} (cm^3 $molecule^{-1}$ sec^{-1}) to 2×10^{-15}, they needed to be at least 5×10^{-13} to match the smog chamber data. At about the same time Weinstock [1969] argued, based on carbon isotope studies, that tropospheric CO had a short lifetime (~0.2 year) and that most of its destruction must occur in the troposphere. One of the suggested destruction paths was OH oxidation (R2), but no general tropospheric source of OH was known.

Motivated by Weinstock's 1969 paper, Levy [1971] constructed a O_3-H_2O-CO-CH_4-NO_X photochemical mechanism for the background or clean troposphere which combined: 1. The $O(^1D)$ production of OH (R1) from the stratosphere with tropospheric H_2O levels; 2. The Heicklen, Westberg and Cohen catalytic OH–HO_2 cycle, the known NO_X oxidation chemistry, and the CH_4 oxidation cycle; and 3. Existing "measurements" of background surface NO_X levels of a few ppbv. This mechanism predicted for the summertime mid-latitude boundary layer, noon OH concentrations of $\sim 3 \times 10^6$ molecules cm^{-3}, a CO tropospheric lifetime of ~0.2 year, and daytime H_2CO mixing ratios of 2 ppbv. McConnell *et al.* [1971] then extended the mechanism to include the oxidation of H_2CO and predicted a large natural source for CO from the completed CH_4 oxidation path. Chameides and Walker [1973] and Crutzen [1974] next employed the peroxy radical oxidation of NO to NO_2, first devised to explain O_3 formation in smog chambers, to produce a global tropospheric source of O_3 that was fueled by CH_4 and CO oxidation and driven by a NO-NO_2 catalytic cycle. By 1974 the basic tropospheric photochemistry, which predicted OH concentrations of $\sim 10^6$ molecules cm^{-3}, large chemical production of tropospheric O_3, and OH control of CH_4 and CO destruction as well as NO_X conversion to HNO_3, was qualitatively well developed (see a review by Levy [1974] for a summary up to that point). While those early calculations remain remarkably reasonable, the estimates of background NO_X were much too high and the estimated rate coefficients for R4 and R5 were much too low. Fortunately these errors compensated.

For the rest of the 1970s there was a rapid development and quantification of the chemical mechanism and OH's reactive role in the troposphere. Kineticists began to measure many of the key rate coefficients that had previously only been estimated. Most important of these was the measurement by Howard and Evenson [1977], which increased the rate coefficient for R4 from an estimated 5×10^{-13} to a measured 8×10^{-12}. At the same time, sophisticated measurement devices were being developed for the trace gases in the troposphere, the first of which was a chemiluminescence NO instrument that lowered the de-

tection limit to the pptv range and measured background NO_X levels of 0.1 ppbv or less (see McFarland *et al.* [1979] as an example of this development). Attempts to make direct measurements of tropospheric OH also began. Theoretical calculations improved quantitatively with the inclusion of more accurate rate coefficients and increased in complexity with the addition of non-methane hydrocarbon oxidation. A more realistic global picture of OH and its impact on other trace gases was also developing through the use of approximate 2-D global models. It is not possible to accurately capture the explosion of theoretical, laboratory and field studies of tropospheric chemistry during the 1970s and early 1980s in this short introduction. Rather, I have selected a few examples that provide an idea of the evolution of our theoretical and observational understanding during this period: Fishman *et al.* [1979]; Oltmans [1981]; Logan *et al.* [1981]; Gregory *et al.* [1985]; Beck *et al.* [1987]; Liu *et al.* [1987]; Fehsenfeld *et al.* [1988]; Crutzen [1988].

The following articles examine the current state of our understanding of tropospheric OH and its role in tropospheric chemistry. William Brune discusses our current understanding of OH chemistry and its interactions with NO_X and O_3. Hans-Peter Dorn and Andreas Hofzumahaus review the current state of local OH measurements and their intercomparison with photochemical models. Ivar Isaksen focuses on the important relationship between OH and CH_4 and the impact of this relationship on our current understanding of CH_4 sources and lifetime. Leonid Yurganov examines the role of OH in the current inter-annual variations and trends in CO. And Yuhang Wang reports on recent measurement and modeling studies that attempt to constrain global tropospheric OH concentration and its past and future trends.

Editor's Note: Reference lists have been omitted from all articles due to space limitations. They are available on the IGAC website (http://web.mit.edu/igac/www) or in hardcopy upon request from the IGAC Core Project Office (igac@mit.edu; Fax: +1–617–253–9886).

OH and HO_2: Sources, interactions with nitrogen oxides, and ozone production

Contributed by **William Brune** (brune@essc.psu.edu), *Pennsylvania State University, USA.*

Hydrogen oxides and nitrogen oxides are two basic components of atmospheric chemistry. Hydrogen oxides (HO_X) consist of the hydroxyl radical (OH) and the hydroperoxyl radical (HO_2). Nitrogen oxides (NO_X) consist of nitric oxide (NO) and nitrogen dioxide (NO_2). Together they determine the atmosphere's oxidizing, or cleansing, power and the troposphere's ozone production.

OH and HO_2 concentrations typically increase during the day and are larger in polluted environments than in clean ones. Two factors are responsible for most observed HO_X variance: the HO_X production rate, denoted as $P(HO_X)$, and the NO_X concentration [Logan *et al.*, 1981; Ehhalt *et al.*, 1991; Jaeglé *et al.*, 1999, 2000a]. Reactions that destroy HO_X are also important, but as we shall show, the dominant HO_X-destroying reactions are basically determined by the HO_X production rate and the NO_X concentration. In this article, we discuss the production of OH and HO_2, the interactions between HO_X and NO_X that establish the OH and HO_2 concentrations and the ozone production rate, $P(O_3)$, and the lessons garnered from a growing body of atmospheric measurements of OH and HO_2.

The production of OH and HO_2

Globally the most important HO_X source is the photodestruction of ozone to produce the excited state oxygen atom, $O(^1D)$, which reacts with water vapor to produce two OH molecules [Levy, 1971]. It is by far the largest HO_X source in the lower troposphere. However, in the upper troposphere and in some continental environments, other sources can be important and indeed dominant. Some of these other sources are made elsewhere by oxidation processes initiated by the reaction of OH with a hydrocarbon. They are then transported to a new location where they become important or dominant HO_X sources (Figure 1). The convection associated with clouds appears to be effective at lifting HO_X sources from planetary boundary layer (~0.5-2 km) to the middle and upper troposphere [Prather and Jacob, 1997]. These HO_X sources become more important than $O(^1D)+H_2O$ above ~6 km altitude. Precursor gases to these HO_X sources may also be lifted by convection. Thus, pollution from megacities and biomass burning, lofted into the upper troposphere, can become the dominant HO_X source and result in efficient ozone production. It can also be transported great distances before descent, possibly influencing the chemistry of remote regions.

Several of these convectively lifted gases that have origins near Earth's surface have been identified. They include acetone ($CH_3C(O)CH_3$) [Singh *et al.*, 1995; Arnold *et al.*, 1997], methylhydroperoxide (CH_3OOH) [Prather and Jacob, 1997; Cohan *et al.*, 1999], and formaldehyde (CH_2O) and other aldehydes [Müller and Brasseur, 1999]. Hydrogen peroxide (H_2O_2) is another source [Chatfield and Crutzen, 1984], but it is so water soluble that it is probably scavenged by precipitation as it is drawn up through clouds. All of these chemical species produce OH or HO_2 after they have been destroyed by sunlight. For acetone and methylhydroperoxide, the photodestruction leads to production of formaldehyde (CH_2O), which is

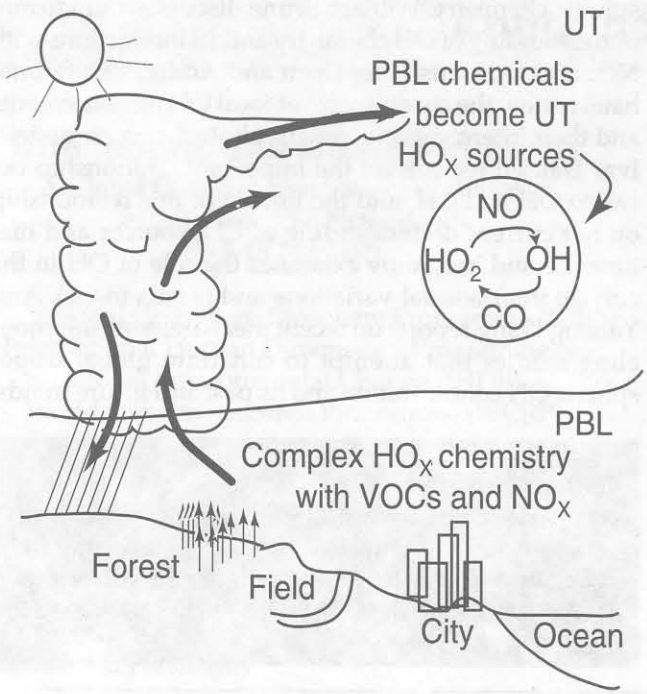

Figure 1. Schematic of tropospheric HO_X photochemistry. Complex chemistry in Earth's planetary boundary layer (PBL) produces oxygenated species. These can be convectively lifted into the upper troposphere (UT), where they become HO_X sources. In the UT, HO_X is exchanged between HO_2 and OH by reaction of HO_2 with NO and OH with CO. The reaction of HO_2 with NO leads to O_3 production.

rapidly destroyed by sunlight to produce HO_2. Other as-yet-unidentified source gases are also likely lifted from the surface into the upper troposphere [Crawford *et al.*, 1999], especially in convection over continents.

Another HO_X source is the reaction of OH with methane [Logan *et al.*, 1981; Wennberg *et al.*, 1998]. This reaction initiates an oxidation process that eventually produces water vapor and carbon dioxide. Even though OH is destroyed in the initial reaction with methane, generally more HO_X is produced than destroyed. This behavior is called autocatalytic. The amount of HO_X produced depends on the amount of NO present, but for much of the atmosphere, this autocatalytic process produces a net ~0.6 HO_X molecules for every methane and OH molecule initially consumed.

For larger non-methane hydrocarbons, such as those found in urban areas and forests, the oxidation pathways can be much more complex than for those of methane [Trainer *et al.*, 1987]. After the initial reaction between OH and these volatile organic compounds (VOCs), RO_2 soon forms, where R is a hydrocarbon radical. Formation of RO_2 often leads to formation of HO_2. Whether the oxidation of a particular hydrocarbon is a net HO_X source or sink depends on a number of factors, particularly the amount of NO present. While VOCs are certainly important for the chemistry in Earth's planetary boundary layer, where people live, they may have a more global role if they are carried to the upper troposphere.

Because HO_X production, $P(HO_X)$, is generally driven by sunlight, we would expect that OH and HO_2 exist only during daylight. However, HO_2 has been observed to persist through the night at levels of a few parts per trillion by volume (1 pptv = 10^{-12} molecules per total molecules in the air). Such observations point to possible nighttime HO_X sources, such as OH production in the reaction between ozone (O_3) and certain terpenes [Paulson and Orlando, 1996]. While measurements hint at such sources [Kanaya *et al.*, 1999; Hard *et al.*, 1992], observations have not firmly established their presence. Even if these sources exist, their impact on even regional chemistry is uncertain.

The roles of NO_X and $P(HO_X)$ in HO_X photochemistry

Some HO_X sources create OH; some create HO_2 (Figure 2). Once created, HO_X is partitioned within seconds into OH and HO_2 by a few fast reactions. The reaction of OH with CO, volatile organic compounds (VOCs), ozone, and other chemicals produce HO_2. Similarly, reactions of HO_2

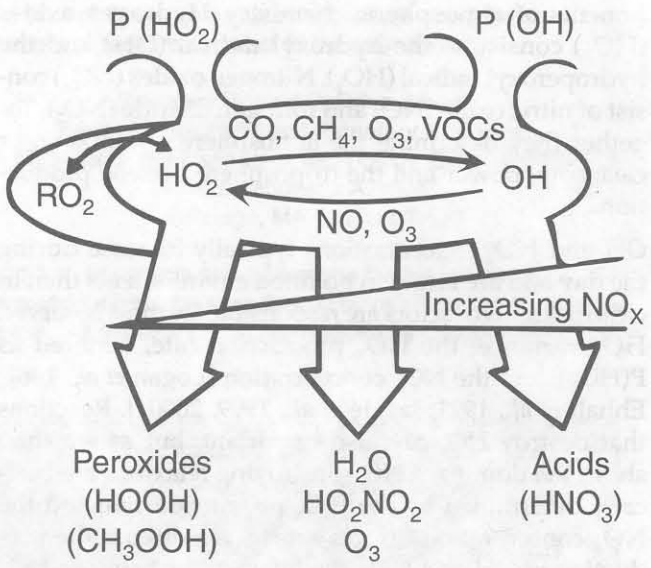

Figure 2. Schematic of the influence of NO_X and $P(HO_X)$ on HO_X photochemistry. HO_X is produced as either OH or HO_2, is rapidly exchanged between HO_2 and OH, creating O_3 in the process, and is removed by reactions that eventually form H_2O. The dominant removal reactions are determined by the NO_X abundance and the HO_X production rate.

with NO and O_3 produce OH. Throughout much of the atmosphere, the production of OH and HO_2 through these reactions is much faster than the OH and HO_2 production from other sources. When this is true, the interchange between OH and HO_2 comes into steady-state relative to the production and destruction of HO_X (i.e., the OH and HO_2 concentrations maintain a balance with each other, but the total HO_X concentration adjusts to the changing environmental conditions, such as sunlight).

The dominant reactant with OH is usually CO, although other species can be important. In forested regions, the dominant reactant with OH is often isoprene, a 5-carbon molecule that is emitted mostly by deciduous trees. In urban environments, the dominant reactant can be oxygenated species, particularly formaldehyde and other aldehydes.

The relative rates of reaction of OH with CO, VOCs, and O_3 and HO_2 with NO and O_3 determine how much HO_X is OH and how much is HO_2. The greater the amount of CO or VOCs, the more HO_2 there is relative to OH. With rare exceptions, the concentration of HO_2 is more than five times greater than the concentration of OH and is usually 10's to 100's of times larger.

During the cycling between OH and HO_2, O_3 is produced. Ozone production occurs when HO_2 and RO_2 react with NO to form OH (or RO) and NO_2. The NO_2 is rapidly destroyed by sunlight into NO+O, and the O atom rapidly reacts with O_2 to make O_3. On the other hand, the production of HO_X can destroy O_3, as can the reactions of OH and HO_2 with O_3. Thus the net ozone production is dictated by the expression:

$$d[O_3]/dt = \{k_{HO2+NO}[HO_2]+k_{RO2+NO}[RO_2]\}[NO]$$
$$- \{J_{O3}f[H_2O] + k_{OH+O3}[OH] + k_{HO2+O3}[HO_2]\}[O_3]$$

where [OH] is the OH concentration, k_{X+Y} is the reaction rate coefficient for X+Y → products, and $J_{O3}f[H_2O]$ is the production rate of $O(^1D)$ times the fraction that react with H_2O. The level at which NO becomes more important than O_3 depends on the [NO] and [O_3] [Crutzen, 1979]. For typical [O_3] values, it occurs when the NO mixing ratio exceeds a few tens of pptv.

HO_X is permanently lost when its hydrogen atom is recombined into water vapor. HO_X can be destroyed by several reactions, although the relative importance of the different reactions depends on the amount of NO_X present (Figure 2). At low NO_X, HO_2 is hundreds of times more abundant than OH. Most HO_X loss occurs by HO_2 reactions with either HO_2 or RO_2 (R = CH_3 or other hydrocarbon radicals denoted as R) to form peroxides (HOOH, CH_3OOH, ROOH). Peroxides do not represent a permanent HO_X loss because they can be destroyed by sunlight to produce HO_X again. For conditions in which the peroxide sources and sinks come into steady-state,

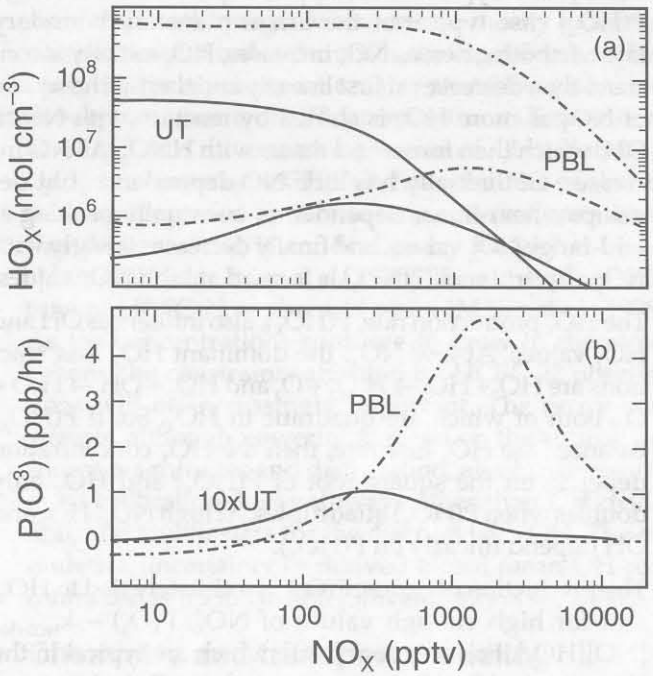

Figure 3. (a) HO_X concentrations and (b) O_3 production rates as a function of NO_X for conditions in the upper troposphere, UT (solid line), and planetary boundary layer, PBL (dashed line). In (a), the higher lines are HO_2 and the lower lines are OH at low NO_X. In (b), $P(O_3)$ in the UT is multiplied by 10. For the UT, $P(HO_X) = 2.5 \times 10^4$ molecules cm^{-3} s^{-1}; for the PBL, $P(HO_X) = 2.5 \times 10^6$ molecules cm^{-3} s^{-1}.

HO_X is lost when OH reacts with the peroxides to produce H_2O.

At low levels of NO, below a hundred pptv in remote areas and below a thousand ppbv in polluted urban areas, NO shifts HO_X from HO_2 to OH, so that the fast reaction $OH+HO_2 \rightarrow H_2O+O_2$ becomes an important loss as OH increases. At the same time, sufficient NO_2 usually exists in photostationary state with NO that pernitric acid, HO_2NO_2, is formed by the reaction $HO_2+NO_2+M \rightarrow HO_2NO_2+M$, where M is an air molecule. Pernitric acid is unstable to both sunlight and thermal decomposition; its production and loss often balance, so that it is neither a HO_X source nor sink. Its main loss is by reaction with OH to produce H_2O.

Finally, at high NO_X, HO_X is increasingly shifted from HO_2 to OH. The increased OH reacts with NO_2 to form nitric acid (HNO_3). Nitric acid is only slowly destroyed by sunlight and may be removed by rapid scavenging by aerosols, cloud drops, and rain drops. For much of the atmosphere, it is permanently removed by reaction with OH to produce H_2O.

The concentrations of OH and HO_2, and ozone production, $P(O_3)$, display this strong dependence on NO_X, as in Figure 3. Two midday cases are presented: a low

$P(HO_X)$ case typical of the upper troposphere and a high $P(HO_X)$ case typical of the urban planetary boundary layer. In both cases, as NO_X increases, HO_2 initially is constant, then decreases at first linearly and then as the square of NO_X as more HO_X is shifted by reaction with NO to OH, which then forms and reacts with HNO_3. As NO increases, OH initially has little NO dependence, but develops a near-linear dependence, eventually peaking at mid-range NO_X values, and finally decreases linearly with NO_X as nitric acid (HNO_3) is formed at high NO_X values.

The HO_X production rate, $P(HO_X)$, also influences OH and HO_2 values. At low NO_X, the dominant HO_X loss reactions are $HO_2 + HO_2 \rightarrow H_2O_2 + O_2$ and $HO_2 + OH \rightarrow H_2O + O_2$, both of which are quadratic in HO_X. So, if $P(HO_X)$ balances the HO_X loss rate, then the HO_X concentration depends on the square root of $P(HO_X)$ and HO_X only doubles when $P(HO_X)$ quadruples. At high NO_X, HO_2 and OH depend linearly on $P(HO_X)$.

The production of ozone, $P(O_3)$, is intimately tied to HO_X, and for high enough values of NO_X, $P(O_3) \sim k_{HO2+NO}[NO][HO_2]$. For very low [NO], which are typical in the clean tropical Pacific lower troposphere, O_3 is destroyed [Schultz et al., 1999]. As NO_X increases, $P(O_3)$ increases almost linearly with NO_X, reaches a peak when HO_2 becomes proportional to $[NO_X]^{-1}$, and then decreases linearly with NO_X as HO_2 decreases as the square of NO_X. The peak in the ozone production shifts to higher NO_X as $P(HO_X)$ increases.

If $P(O_3)$ increases as NO is increased, then ozone production is said to be NO_X-limited. If $P(O_3)$ is constant or decreases as NO_X is increased, then ozone production is said to be NO_X-saturated. Whether a region of the atmosphere is NO_X-limited or NO_X-saturated is an important question for determining the impact of future human pollution, particularly NO_X, on that region.

Observational tests of HO_X photochemistry

How well do the observations fit this basic picture of HO_X and its relationship with NO_X? One test is the comparison of observed HO_X to models that are constrained by simultaneous measurements of other chemical species and environmental parameters. Field studies have sampled environments with wide ranges of NO_X and $P(HO_X)$. In general, the daytime observations agree to within a factor of two or better with models that are tightly constrained by a large number of simultaneous measurements of other chemical species and environmental parameters. Considering the range of conditions sampled, this level of agreement is remarkable. Despite this general good agreement, some disagreements persist. The ways that observations and models disagree are different for different regions.

In the upper troposphere, observations are sometimes greater than model values, implying that additional HO_X sources are not being measured [Wennberg *et al*, 1998; Jaeglé *et al*, 1997; Brune *et al.*, 1998]. It is presumed that these source species were acetone and methylhydroperoxide, which were not measured during these studies. Neither the global extent of their importance nor the possibility of other sources is known.

Near Earth's surface, observed OH and HO_2 have generally been equal to or less than modeled OH and HO_2 by as much as a factor of 0.7 [Plass-Dülmer *et al.*, 1998; Eisele *et al.*, 1996; Mount and Williams, 1997; Frost *et al.*, 1999]. Even though the deviation of the observations from the models is within the combined uncertainties, it has occurred in enough environments to be troubling. Proposed causes for the deviations include OH reactions with unmeasured hydrocarbons and HO_2 loss on aerosols.

In the upper troposphere over the North Atlantic, recent measurements suggest an NO dependence of the deviation between measured and modeled HO_X [Brune *et al.*, 1999; Faloona *et al.*, 2000]. HO_X observations are about 60% of the model values for NO less than a hundred pptv and increase to roughly twice the model values at NO values exceeding a few hundred pptv. This effect is seen for both OH and HO_2. At the same time, observations and models give the same HO_2/OH ratio. It is not understood what is causing this NO-dependent discrepancy. It may be that additional HO_X sources accompany the increased NO_X or that the photochemical interactions between HO_X and NO_X are not well understood for the cold, upper troposphere. These problems could involve pernitric acid (HO_2NO_2) or nitric acid (HNO_3) formation or destruction.

No matter what the cause for the NO-dependency, these observations suggest that more of the atmosphere is NO_X-limited than models calculate and that it remains NO_X-limited to higher values of NO_X. Currently, models calculate that the upper troposphere would quickly become NO_X-saturated if much more NO_X were added. In other field studies in the upper troposphere, NO_X-limited conditions are also observed more frequently than calculated by models [Jaeglé, 2000b]. If this is true, then increases in pollution from biomass burning, urban smog, or aircraft could produce more O_3 than expected.

Challenges lie ahead. Measuring the dependence of OH, HO_2, and $P(O_3)$ on varying NO_X and $P(HO_X)$ a few times in a few places is not enough. The fundamental properties of atmospheric chemistry must be examined in several environments, such as cities, forests, the marine boundary layer, and the free troposphere. They must be studied with different HO_X instrumentation to ensure that the observations are real. Only then will we be able to develop confidence in the understanding of atmospheric oxidation and ozone production and to reduce the potential for surprises in chemical mechanisms.

Measurement methods for atmospheric OH

Contributed by **Hans-Peter Dorn** (h.p.dorn@fz-juelich.de) *and* **Andreas Hofzumahaus** (a.hofzumahaus@fz-juelich.de), *Forschungszentrum Jülich, Institut für Atmosphärische Chemie, Germany.*

The hydroxyl radical (OH) is the major oxidizing agent in the atmosphere. Chemical reactions with OH initialize the removal of carbon monoxide (CO), methane (CH_4), and volatile organic compounds (VOC). The OH required for these oxidation processes is produced everywhere in the sunlit atmosphere by UV photo dissociation of ozone (O_3) and subsequent reaction of the emerging $O(^1D)$ with water vapor:

$$O_3 + h\nu(<340nm) \rightarrow O(^1D) + O_2 \qquad (R1)$$

$$O(^1D) + H_2O \rightarrow OH + OH \qquad (R2)$$

Reactions with OH initialize chain reactions, which eventually lead to a removal of the oxidized species from the atmosphere. Since Levy [1971] first postulated this basic concept of tropospheric photochemistry, numerous estimates of the globally averaged OH concentration have been obtained from the budget of species that are exclusively removed by reaction with OH and for which the source strengths are well known (e.g., ^{14}CO, CH_3CCl_3). The most recent of these studies yielded concentrations close to $1x10^6$ OH/cm^3 [Prinn *et al.*, 1995; Krol *et al.*, 1998; Spivakovsky *et al.*, 2000].

Why should we measure OH locally?

The global mean OH controls the atmospheric lifetimes of trace gases like CH_4 and CO, which are relatively well mixed on a global scale. It can also be viewed as a measure for the self-cleansing capacity of the atmosphere. However, global OH is not a representative quantity on a regional or local scale, for example, polluted or forested areas. In fact, due to the short lifetime resulting from its high chemical reactivity, OH is highly variable in space and time.

The natural variability of OH and its response to atmospheric parameters can be studied only by local measurements at high time resolution. Variations of OH mainly reflect the influence of chemical processes that control the transformation of other important gases and eventually initiate the production of tropospheric ozone or particles. Accordingly, local OH measurements constitute a valuable tool for the direct observation of chemical processes in the atmosphere and for testing our understanding of photochemistry models for different meteorological situations and trace gas burdens.

The challenge of measuring OH

Since the importance of atmospheric OH was recognized in the early 1970s, many intensive efforts (primarily in the U.S. and Germany) were undertaken to measure its concentration on a local scale [see reviews by Crosley, 1994, 1995]. Many of the early OH instruments suffered from insufficient sensitivities and interferences from other gases [Crosley and Hoell, 1986; Beck *et al.*, 1987]. This is not surprising in view of the high demands of measuring atmospheric OH:

1. Its high reactivity in the gas phase and on surfaces places severe practical constraints on instruments that use sampling inlets.
2. The extremely small concentration of typically less than 10^7 OH/cm^3 requires a very high detection sensitivity.
3. High specificity is needed to avoid interferences with trace gases that are much more abundant than OH.
4. An OH concentration standard is not easily available for instruments that require calibration.

In the stratosphere, early measurements were successful [e.g., Anderson, 1976; Heaps and McGee, 1985; Stimple and Anderson, 1988] but lacked simultaneous measurements of other trace gases required to test photochemical theories. Comprehensive sets of simultaneous measurements of OH and trace gases were first obtained in the planetary boundary layer. Although the temporal and spatial resolution of the first field measurements of OH were relatively low, they allowed first tests of tropospheric photochemistry models [Perner *et al.*, 1987; Poppe *et al.*, 1994].

It took roughly twenty years from the first attempts to measure tropospheric OH until, in the first half of the 1990s, experimental techniques achieved the desired reliability, sensitivity, and temporal-spatial resolution to enable systematic measurements of OH in different parts of the world, on the ground, on aircraft, and on ships. While many of the experimental problems of OH detection now seem to be solved, even the most recent OH instruments are technically complex and their deployment in the field is still not trivial.

Current measurement methods

Different techniques have been used for the successful detection of atmospheric OH. These can be grouped into two categories: direct methods, which use optical spectroscopy for OH detection, and indirect methods, which convert OH chemically into another species that can be detected with high sensitivity and specificity. An overview of most of the recent techniques can be found in *Journal of the Atmospheric Sciences* [**52**, 3297-3441, 1995].

Absorption spectroscopy

Differential optical absorption spectroscopy (DOAS) uses the UV absorption lines of OH at 308 nm from transitions between rotational levels of the electronic ground-state (X^2P, $v''=0$) and the first electronically excited state (A^2S^+, $v'=0$). Usually a laser beam is transmitted through

a 1-10 km path in the open atmosphere and the absorption spectrum is detected. The application of Lambert-Beer's law directly yields the OH concentration from the measured absorption. The great advantage of this method is that the required absorption cross-section can be calculated from well known spectroscopic properties of the OH molecule to within better than 10%. Thus, no additional calibration is required [Mount, 1992; Dorn *et al.*, 1995a, Hausmann *et al.*, 1997].

Different configurations of the absorption light-path have been used, either as a double-pass over a long distance (10 km) [Mount, 1992], or as multi-pass where the light beam was folded more than 100 times between the mirrors of an open White cell (total light path length 1-4 km) [Armerding *et al.*, 1994; Dorn *et al.*, 1995b]. The latter configuration enables local OH measurements by absorption spectroscopy and is fairly mobile. Recently a folded-path system was used to measure OH onboard a ship [Brauers *et al.*, submitted to *Journal of Geophysical Research*].

Detection limits of $8 \cdot 10^5$ OH / cm^3 (1σ) were demonstrated in field experiments using a folded light path of 1800 m total length and a time resolution of 200 s [Brandenburger *et al.*, 1998].

Laser-induced fluorescence (LIF)

All LIF instruments used for tropospheric OH detection apply the **F**luorescence **A**ssay with **G**as **E**xpansion (FAGE) concept which was pioneered by Hard, O'Brien and coworkers [Hard *et al.*, 1984; Chan *et al.*, 1990; Hard *et al.*, 1995]. Ambient air is expanded though a nozzle into a low-pressure (1-5 mbar) fluorescence cell. OH radicals present in the resulting gas beam are excited using a narrow-band pulsed laser and are directly detected via their fluorescence. As in the case of DOAS, LIF takes advantage of the discrete UV line absorption spectrum ($A^2S^+ \leftarrow X^2P$) for the selective excitation of OH [Stevens *et al.*, 1994; Heal *et al.*, 1995; Holland *et al.*, 1995; Hard *et al.*, 1995].

In contrast to DOAS, the LIF technique needs to be calibrated. The accuracy obtained with current techniques is about 20%. Even after years of development it is still a difficult task to generate known concentrations of OH at ambient conditions to calibrate the instruments in the field [Holland *et al.*, 1998]. Typical detection limits for 1 minute measurement time are about $(4\text{-}7) \cdot 10^5$ OH / cm^3 (2σ) allowing a good time resolution at a sufficient sensitivity to investigate the natural variability of OH.

The LIF technique can be extended to the *in situ* measurement of HO_2 radicals [Hard *et al.*, 1995]. Their detection is realized indirectly by adding an increment of NO at the inlet of the fluorescence chamber to convert a certain amount of HO_2 into OH.

$$HO_2 + NO \rightarrow OH + NO_2$$

The efficiency of this titration reaction must be regularly controlled by calibration measurements.

Current LIF instruments are compact and robust enough to be used on aircraft and a number of measurements of OH radicals in the free troposphere were conducted in recent years [Brune, this issue; Wang, this issue].

LIF instruments used for measurements in the stratosphere use excitation at 282 nm into the first excited vibrational level of the upper electronic state (A^2S^+, (v'=1)) of OH [Wennberg *et al.*, 1995]. The use of this technique for tropospheric OH is impeded by laser induced production of OH radicals in the detection chamber at 282 nm [Hard *et al.*, 1995].

Chemical conversion techniques

In the past few years three indirect techniques have been applied for OH detection:

Radiocarbon technique

Ambient air is drawn into a UV-transparent flow reactor, to which a small quantity of ^{14}CO is added. A fraction of ^{14}CO is oxidized to $^{14}CO_2$ which is then collected, purified, and analyzed for ^{14}C by gas-proportional counting. The amount of $^{14}CO_2$ is related to the OH concentration through the CO+OH reaction constant and the residence time in the reactor [Felton *et al.*, 1990]. While straightforward in principle, this technique is experimentally challenging and needs long counting times for low OH concentrations.

Liquid phase scrubbing

A potentially new indirect OH measurement method has emerged recently. The advantages are its experimental simplicity, portability, and low expense. The atmospheric OH signal is related to a compound produced by liquid phase reaction of scavenged OH with salicylic acid [Chen and Mopper, 2000]. The reaction product is separated and quantified by HPLC with fluorescence detection. Although still under development, early field studies seem to indicate the feasibility of this approach for OH measurements in clean air. Taking a sampling period of 45-90 minutes, the expected detection limit is estimated to be $(3\text{-}6) \cdot 10^5$ OH / cm^3.

Selected Ion Chemical Ionization Mass Spectrometry (SICIMS)

Ion-assisted OH measurements are performed by pulling ambient air into a flow tube reactor. The central part of the airflow is sampled and OH present is almost quantitatively converted to $H_2{}^{34}SO_4$ by addition of an excess of isotopically labeled $^{34}SO_2$ [Eisele and Tanner, 1991; Tanner *et al.*, 1997]. Ionization is achieved by reaction of $H_2{}^{34}SO_4$ with *in situ* generated $NO_3^-(HNO_3)$ ions further downstream of the reactor. The product ion $H^{34}SO_4^-$ is specifically detected in a quadrupole mass spectrometer with high sensitivity allowing discrimination from the $H^{32}SO_4^-$ signal originating from naturally occurring $H_2{}^{32}SO_4$.

In the past few years this technique was further developed and successfully used during several aircraft campaigns (ACE 1, PEM-Tropics A / B).

SICIMS has a very low detection limit of $2 \cdot 10^5$ OH/cm^3 (2σ) with a fast time response of 30 s. As in the case of LIF, calibration to obtain the absolute concentrations is a challenge. The total systematic error of the ground-based instrument is about 30% [Tanner *et al.*, 1997] whereas the accuracy of the aircraft instrument is 40-60% demonstrating the experimental difficulties to calibrate the instrument for different flight altitudes [Mauldin *et al.*, 1997, 1998, 1999].

Intercomparison of OH instruments

Increasing confidence in the validity of OH field measurements has been gained from a number of intercomparison exercises. The results of the two most comprehensive campaigns, *THOPE* [Tropospheric OH Photochemistry Experiment, 1993], performed in the US (1993), and *POPCORN* [Photo-Oxidant Formation by Plant Emitted Compounds and OH Radicals in North-Eastern Germany, 1994], carried out in Germany [1994] are summarized in special issues of *J. Geophys. Res.* [**102**, 6169-6510, 1997] and *J. Atmos. Chem.* [**31**, 1-246, 1998], respectively.

During THOPE the OH concentrations observed with SICIMS and DOAS agreed within the instrumental uncertainties when clear days and low-NO_X conditions were selected for comparison [Mount *et al.*, 1997]. On average, the SICIMS data were 20% lower than the absorption measurements, which can be explained by different air masses being sampled by the SICIMS point measurements and over the DOAS light path extending over 10 km length.

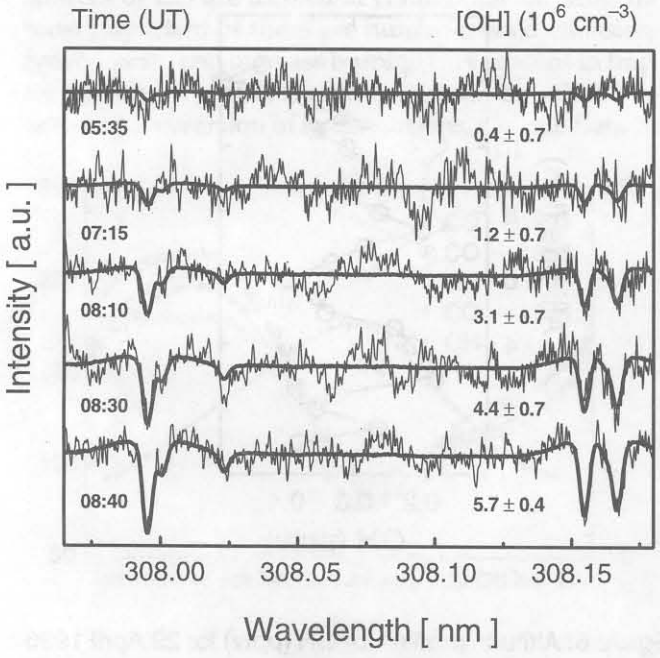

Figure 1: Atmospheric absorption spectra measured using DOAS as a function of time of day (UT). Solid lines are reference absorption spectra of OH radicals fitted to the measurements (Adapted from Brandenburger *et al.*, 1998).

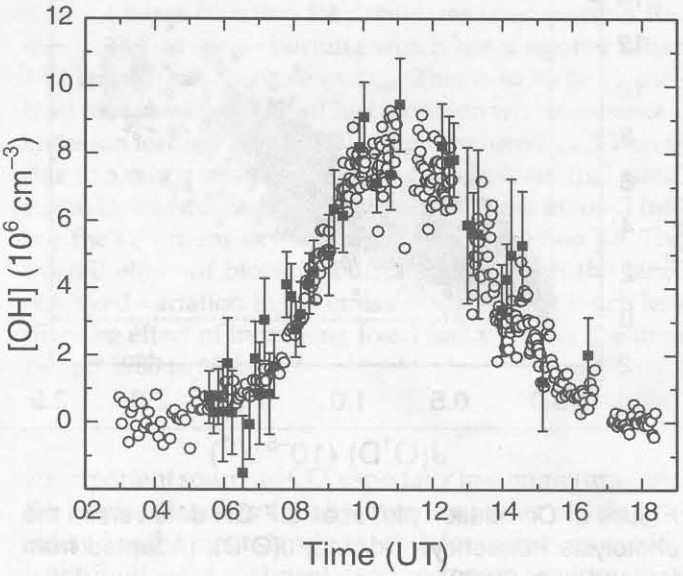

Figure 2: Diurnal variation of OH measured using LIF (o) and DOAS (■) during POPCORN (Adapted from Hofzumahaus *et al.*, 1998).

During POPCORN DOAS LIF and folded-path DOAS instruments were compared. The absorption instrument provided the spectroscopic evidence (Figure 1) that, in fact, hydroxyl radicals were measured [Brandenburger *et al.*, 1998]. Figure 2 shows a diurnal profile of OH measured by LIF and folded-path absorption. The agreement is, in most cases, excellent [Brauers *et al.*, 1996; Hofzumahaus *et al.*, 1998].

Verification of the fundamental properties of atmospheric OH by direct field measurements

To test our understanding of the chemical system controlling OH, it is necessary to have measurements of OH concentrations along with measurements of those parameters that are known to control OH. The new generation of instruments has yielded large OH data sets comprising measurements in different environments. They can be used to test fundamental properties of atmospheric chemistry.

Figure 2 illustrates the dependence of the OH concentration on the solar UV flux. Starting from nighttime concentrations below the detection limit (5×10^5 cm^{-3}) OH reaches its maximum (typically in the range (2-10)$\times 10^6$ cm^{-3} in summer) at local noon when photolysis peaks.

It is clearly demonstrated in Figure 3 that the photolysis of ozone, yielding O(^{1}D), indeed constitutes the domi-

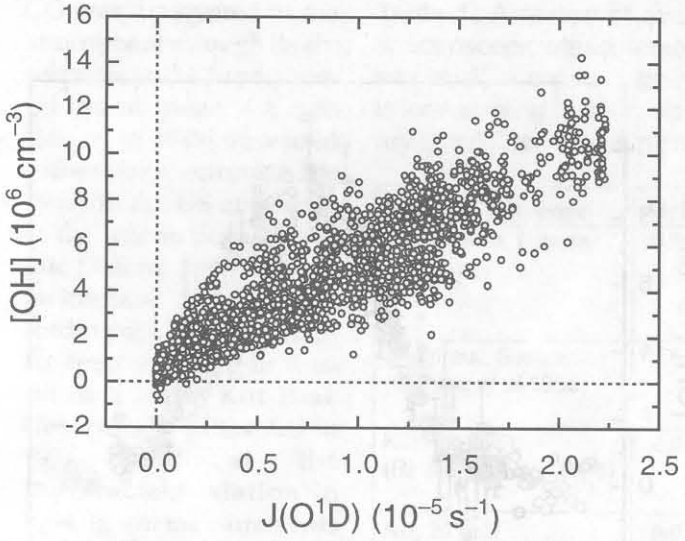

Figure 3: Correlation plot of all LIF OH data versus the photolysis frequency of ozone, J(O^{1}D). (Adapted from Holland *et al.*, 1998).

nant parameter controlling the diurnal variation of OH (see contribution by W. Brune, this issue). Here all OH measurements made during POPCORN are correlated with concurrently measured ozone photolysis frequencies, J(O^{1}D) [Holland *et al.*, 1998; Ehhalt, 1999; Ehhalt and Rohrer, 2000]. The resulting correlation coefficient r^2 = 0.83 indicates that more than 80% of the total variation in OH can be explained by the variation of J(O^{1}D).

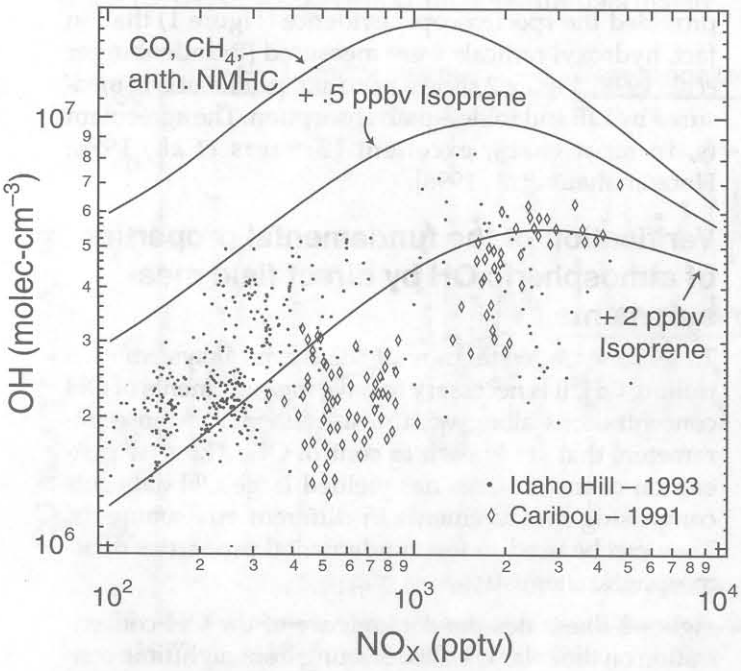

Figure 5: Comparison of observed and calculated OH concentrations versus NO_x during the 1993 Idaho Hill experiment (THOPE). The different model calculations account for different amounts of unmeasured biogenic hydrocarbons [Adapted from McKeen *et al.*, 1997].

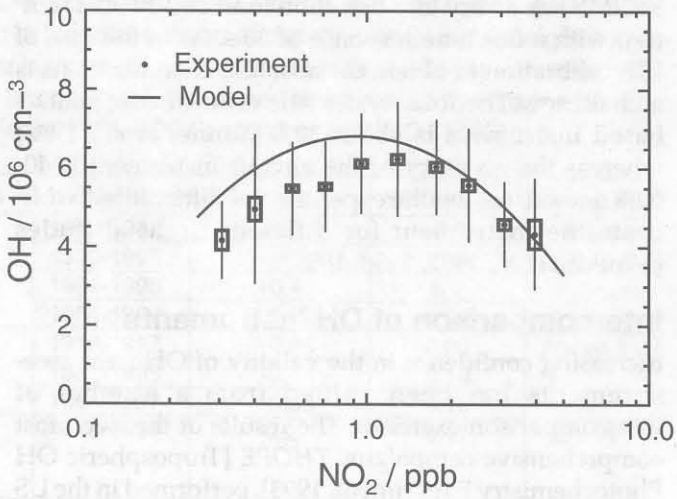

Figure 4: Dependence of the measured OH concentration on NO_2 during the POPCORN field campaign. To make this behavior visible, the OH data were first normalized with respect to J(O^{1}D) and then plotted versus equal log(NO_2)-intervals of 0.1. Full curve corresponds to the model-calculated dependence. [Adapted from Ehhalt, 1999].

The non-linear dependence of OH on NO_x, which represents the next most important control factor, can also be extracted from recent field measurement data (Figure 4).

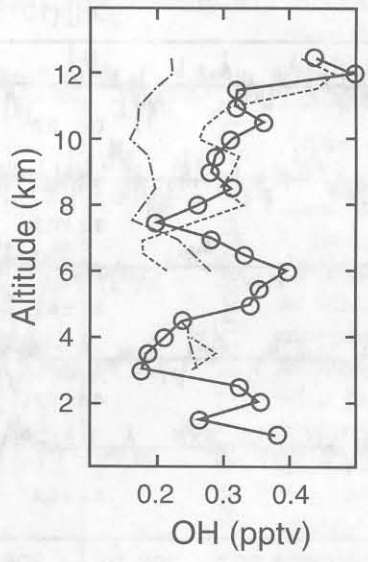

Figure 6: Altitude profiles for OH (pptv) for 29 April 1996 during SUCCESS over Oklahoma. Averaged into 0.5 km altitude bins, observations (circles) are compared to two Harvard University model calculations: using Eppley data to derive albedo (dashed line) and climatology for albedo (dash-dot line). Gaps occur where data are missing. Observational precision is better than 0.03 pptv.

How well do local measurements of OH compare with models?

After experimental confirmation of the two major functional dependencies of OH we have to ask for the quantitative representation of atmospheric OH by models.

Summarizing the results of OH field measurement campaigns carried out in the planetary boundary layer we can state:

1. In clean air masses, good agreement within the combined uncertainties of models and measurements is obtained. On average, the differences observed are 10%-30%, which is very small. However, there are individual cases showing differences up to 50% and more [Mauldin *et al.*, 1998; Ehhalt, 1999; Frost *et al.*, 1999; Brauers *et al.*, data from a recent ship campaign on the Atlantic Ocean, submitted to JGR]. However, all cases have in common that the models tend to calculate higher concentrations.
2. In more polluted air, particularly regions of strong biogenic emissions, the discrepancy is larger, indicating far less understanding of these environments (Figure 5). However, this does not necessarily imply that the models are not capable of describing the more complex chemistry in these environments. Incomplete chemical characterization of the air masses and hence of the chemical processes in the model is most likely the cause of a systematic underestimation of OH loss reactions by models [McKeen *et al.*, 1997].

Moreover, in the continental upper troposphere (above 8 km), a region which is considered clean, OH measurements using LIF exceeded modeled data by factors of 1.5 to 6. The analysis of the observations has suggested that this experimental finding again can be attributed to incomplete measurements of OH source molecules and the resulting lack of these processes in the model applied [Brune *et al.*, 1998; Jaeglé *et al.*, 1998].

Summary

Field measurements of OH have confirmed our understanding of elementary aspects of atmospheric chemistry.

Calculations of the global distribution of OH are consistent within a few percent with the current budgets of well-known tracers [Spivakovski *et al.*, 2000]. On a local basis, however, the chemical system is currently understood to a much lesser extent.

During the past decade many successful field campaigns all over the atmosphere have demonstrated the availability of several different OH measurement techniques with sufficient sensitivity and time resolution. However, in view of many open questions, investigation of atmospheric OH photochemistry is necessary and will remain a further challenge for experimentalists and for modelers.

The atmospheric sink of methane

Contributed by **Ivar S.A. Isaksen** (i.s.a.isaksen@ geofysikk .uio.no), *Department of Geophysics, University of Oslo, Norway.*

Introduction

Loss of atmospheric methane is dominated by the reaction with the hydroxyl radical (OH) in the troposphere:

$$CH_4 + OH \rightarrow CH_3 + H_2O \qquad R1$$

In addition there is minor methane removal through other sinks. Losses that have been suggested are: Absorption in the soil, transport to the stratosphere where methane reacts with OH, Cl and $O(^1D)$, and reaction with Cl in the atmospheric boundary layer. Together these minor sinks account for approximately 10–15 % of the total loss of atmospheric methane. The methane loss rate is therefore first of all determined by the total atmospheric burden of OH and its changes in time.

The total lifetime of atmospheric methane is given by the equation:

$$1/\tau_{CH4} = 1/\tau_{OH} + 1/\tau_{additional} \qquad (1)$$

The methane lifetime due to the reaction with OH is $\tau_{OH} = 1/(k_1 \bullet [OH])$, where k_1 is the reaction coefficient for R1 and [OH] the concentration of OH. $\tau_{additional}$ denotes the methane lifetime due to the combined minor sinks given above. $\tau_{OH} = 9.6$ years has been obtained by scaling from a methyl chloroform (CH_3CCl_3) lifetime of 5.7 years (Spivakovsky *et al.*, 2000). The total methane lifetime was estimated to be τ_{CH4}=8.4 years. Using this method to estimate methane lifetime implies that any corrections of the methyl chloroform lifetime would lead to changes in the methane lifetime. In fact, from a recent analysis of methyl chloroform observations, Montzka *et al.* [2000] deduced a reduced atmospheric lifetime of methyl chloroform of 5.2 (±0.2-0.3) years. This implies a methane lifetime that is shorter than the one given above.

The atmospheric lifetime of methane is calculated using 3-D tropospheric chemical transport models (CTMs) is estimated to be similar to what was obtained from the methyl chloroform analysis. For instance, the IPCC Assessment of aircraft impact on the atmosphere [Isaksen and Jackman, 1999] reports atmospheric lifetimes of methane in the range 6.6 to 10.5 years for 1992.

The estimated lifetime of 8.4 years gives a total sink for atmospheric methane of 576 Tg/yr. Estimates of the global source strength are typically of the order 580 to 600 Tg/year. This is in agreement with the estimated sinks and increase in atmospheric burden [Hein *et al.*, 1997; Lelieveld *et al.*, 1998; IPCC, 1996]. It should be noted, however, that estimates of sources and sinks are connected with large uncertainties. Hein *et al.* [1997] estimate the total methane emission to be in the range 520

to 625 Tg/yr, while Lelieveld *et al.* [1998] estimate the total sink to be 600 ± 80 Tg/yr. There are equal or larger uncertainties connected to the individual sources; Lelieveld *et al.* [1998] estimate total natural methane emission to be 190 ± 70 Tg/yr, with the largest contribution from wetlands (145 ± 30 Tg/yr). They estimate fossil fuel related emissions to be 120 ± 40 Tg/yr, and agricultural sources to be 230 ± 115 Tg/yr.

Atmospheric abundance of methane has increased approximately by a factor 2.5 since pre-industrial time, and it continues to increase. Concentrations have increased from 1.52 ppm in 1978 to 1.76 ppm in 1998. There is, however, a significant declining trend in the methane increase over the last two decades [Dlugokencky *et al.*, 1998], with large year-to-year variations. The methane growth rate since 1992 has been 4.9 ppb/yr.

Changes in the emission of methane from major sources like wetlands, fossil fuel-related or biomass burning are likely causes for the observed short term, year-to-year growth in atmospheric methane. An atmospheric lifetime of methane of 10 years or less is sufficiently short that changes in the global OH concentration that last a few years will have significant impact on the methane growth rate.

Chemical processes determining the OH distribution and the methane lifetime

The local abundance of OH is determined by the local abundance of source and sink gases: CO, CH_4, O_3, nonmethane hydrocarbons (NMHC), NO and water vapor, as well as the intensity of solar UV-B radiation. Based on the methyl chloroform loss rate in the atmosphere Prinn *et al.*, [1995] and Kroll *et al.* [1998] estimated an average global OH concentration of approximately $1x10^6$ molecules/cm^3. However, the concentration varies significantly over the day, with season, and with geographical location.

The main production of OH (and odd hydrogen) in the troposphere occurs through the photo dissociation of ozone by UV-B radiation followed by the reaction with of exited state oxygen with water vapor:

$$O_3 + h\nu \rightarrow O(^1D) + O_2 \quad (R2)$$

$$O(^1D) + H_2O \rightarrow OH + OH \quad (R3)$$

Changes in tropospheric ozone, UV-B radiation and water vapor will therefore affect the OH distribution. Tropospheric ozone will increase as a result of increased emissions of NO_X, CO, non-methane hydrocarbons (NMHC) and CH_4.UV-B radiation will change as a result of changes in stratospheric ozone and changes in tropospheric water vapor could be caused by climate changes.

Several chemical reactions are involved in the ozone loss in the troposphere. The main loss occurs through the reaction with CO converting OH to HO_2:

$$CO + OH \rightarrow CO_2 + H \quad (R4)$$

$$H + O_2 + M \rightarrow HO_2 + M \quad (R5)$$

Approximately 70% of the global OH loss is estimated to go through this reaction (Karlsdottir and Isaksen, 2000), and approximately 15–20% through the reaction with CH_4 (R1). Additional loss occurs via reactions with CH_2O, NMHC and ozone. The lifetime of OH is very short (less than 1 second).

Conversion from HO_2 through gas phase reactions is important for the tropospheric abundance of OH. The two main reactions are:

$$NO + HO_2 \rightarrow NO_2 + OH \quad (R6)$$

$$O_3 + HO_2 \rightarrow OH + OH + O_2 \quad (R7)$$

One important result of the OH forming and loss reactions given above is that increased emission of carbon monoxide and hydrocarbons lead to reduced OH concentrations and longer methane lifetime. Enhanced emission of NO has the opposite effect. The NO/CO ratio in emissions is therefore more important for the abundance of OH than the absolute emission of the gases.

Since reaction R1 affects the atmospheric lifetime of both methane and OH, increases in methane emission will lead to reduced ozone levels and thereby to a longer atmospheric lifetime of methane (1) which further increases atmospheric concentrations of methane (positive feedback) [Isaksen, 1988; Berntsen *et al.*, 1992]. The methane feedback factor F is given by:

$$\alpha = \Delta[CH_4]/\Delta EM_{CH4} \quad (2)$$

where $\Delta[CH_4]$ is the change in global methane equilibrium concentration for a change in global emission ΔEM_{CH4}. Extensive studies of the feedback factor have been performed over the last 10 years. IPCC (1995) reported values in the range 1.2–1.7 from 2-D and 3-D model studies. In a recent intercomparison between five different 3-D CTMs [Karlsdottir, 2000], values for F in the range 1.34 to 1.63 for atmospheric oxidation by OH were obtained. These studies demonstrate that methane oxidation of OH plays a significant role for atmospheric increase of methane.

Changes in methane lifetime

It is likely that the global OH distribution has changed since pre-industrial time due to increases in precursor emissions (CO, CH_4, NO_X) and ozone. How large the change is is, however, uncertain due to the counteracting effects of CO and CH_4 (reduces OH through reactions R1 and R4, respectively), and NO_X and O_3 (increases OH increases through reaction R6 and R7, respectively). Lelieveld *et al.* [1998] calculate a significant reduction in OH and increase in methane lifetime from pre-industrial time (6.2 yr) to 1992 (7.9 yr), while Berntsen *et al.* [1997] calculate an increase in global OH of approxi-

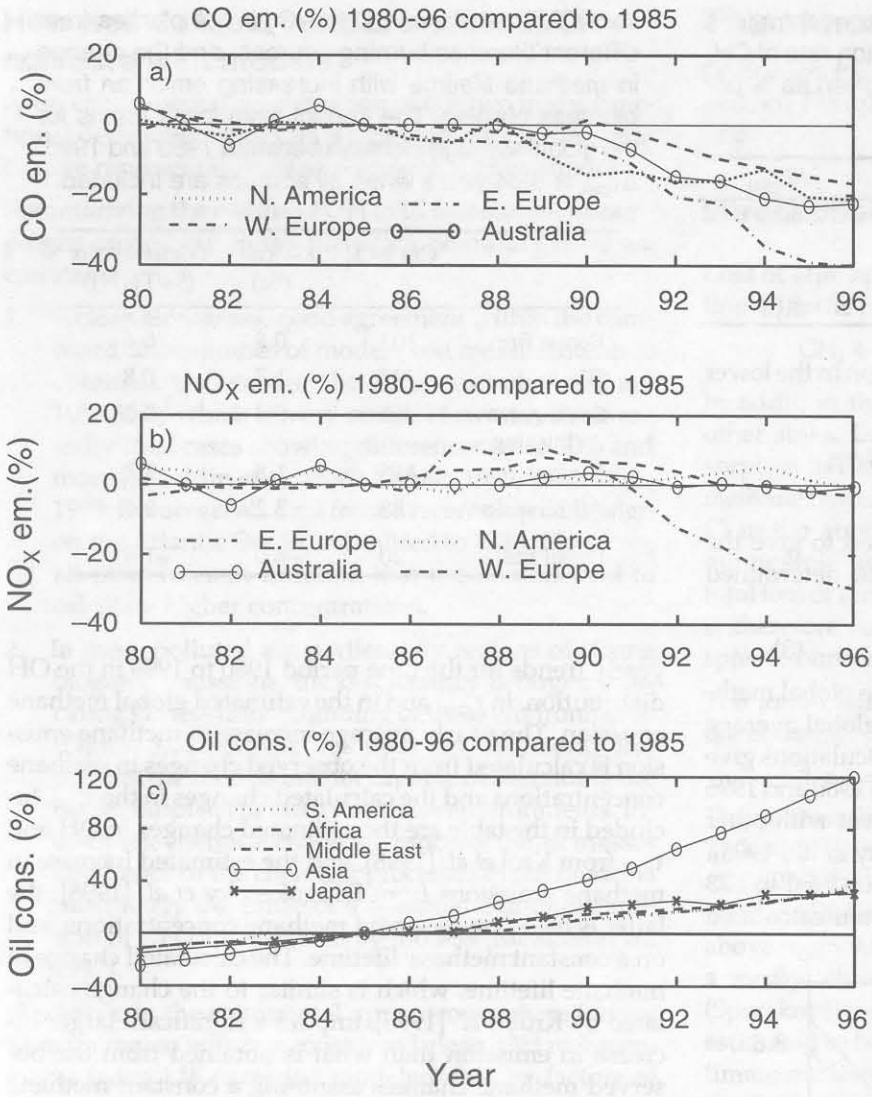

Figure 1. The evolution of the fossil fuel emission of CO (a), NO_x (b), for North America (..), Western Europe (—), Eastern Europe (-.-), and Australia (- o -); and fossil fuel consumption (c) for South America (..), Africa (—), Middle East (-.-), South East Asia (China and India included) (- o -) and Japan (- x -) compared to 1985 values.

mately 6% (and decrease in methane lifetime). Future changes in methane lifetime, particularly toward the end of the 21st century, are highly uncertain due to the large uncertainties in precursor emissions [IPCC, 2001].

We have used the 3-D Oslo CTM1 [Berntsen and Isaksen, 1997] to calculate changes in global OH distribution and methane lifetime for the time period 1980 to 1996 [Karlsdottir and Isaksen, 2000]. We further estimated the implication the changes in lifetime have had for the global methane emissions. Methane changes over the time period were constrained by observations [WMO, 1992; IPCC; 1996: Dlugokencky *et al.*, 1998]. Nine different regions were selected where changes in NO_x, CO and NMHC emissions were given. Figure 1 shows the emission changes for the time period 1980 to 1996 adopted for different regions for CO and NO_x, and for oil consumption. The latter numbers were used to characterize the emissions for developing countries and Japan. References to the adopted emissions are given in Karlsdottir and Isaksen [2000]. There are large differences in the adopted emission trends between the different regions, and in the ratio of the OH production to the OH loss precursors (e.g., NO_x to CO ratio). Eastern Europe had a marked reduction in NO_x emissions during the 1990s, while the rest of the world experienced either small changes in NO_x emissions or significant increases. CO emissions on the other hand, decrease significantly during the 1990s in the industrial regions. This different emission pattern is estimated to have led to significantly different developments in the OH abundance in the different regions.

The calculated trends in the global OH distribution, and in the methane lifetime, are shown in Figure 2. The changes in emissions from fossil fuel usage over the time period considered are estimated to have had a significant impact on the OH distribution, and on the methane lifetime. Of particular importance is the shift in emission pattern from northern industrial regions to developing countries (e.g., South East Asia (SEA) as pointed out by Gupta *et al.* [1998]). We estimate the global average concentrations of OH to have increased from 0.95×10^6 in 1980 to 1.01 molecules/cm^2 in 1996. Different sensitivity studies were performed to estimate the impact of CO and NO_x emissions globally, as well as from SEA sources. In each of the model runs, which were performed for the last year of the period, either the CO or the NO_x emissions were kept constant at the 1985 levels. The results of these sensitivity studies, which are included in Figure 2, reveal that the main contribution to the reduced atmospheric lifetime of methane after 1985 was the rapidly growing NO_x emission in SEA. The increase in CO emission in the same region had some effect on the methane lifetime. NO_x emission increase in SEA since 1985 reduced the methane lifetime by approximately 0.5 years, while CO emission in the same region increased the lifetime by approximately 0.2 years between 1985 and 1996. Emission changes in other regions of the world have had smaller impact on the methane lifetime. There are two reasons for this: Firstly, the rapid growth in anthropogenic emissions in the tropics and, secondly, methane

Table 1. Trends in the global average OH concentrations (Δ OH), CH_4 lifetime ($\Delta\tau_{CH4}$) and the emission rate of CH_4 (ΔP_{CH4}) during the period 1980 to 1996 (given as % per yr).

	ΔOH	$\Delta\tau_{CH4}$	ΔP_{CH4}
This work	0.43	-0.49	0.67
Krol *et al.* [1998]	0.46	-0.45	
Prinn *et al.* [1995]	0.0	0.0	
Dlugokencky *et al.* [1998]			<0.17

lifetime is basically determined by oxidation in the lower troposphere at low latitudes.

Implications for methane emission changes

The global source strength of CH_4 needed to give the observed global CH_4 concentration can be determined by the equation:

$$dC(t)/dt = P(t) - L(t) \times C(t) \qquad (3)$$

C(t) is the concentration of CH_4, P(t) is the global methane emission, and L(t) is the calculated global average loss rate = $1/\tau_{CH4}$ is given by Eq. 1. The calculations give a yearly mean methane emission between 1980 and 1996 of 542.7 Tg/yr, which is in good agreement with other estimates [Fung *et al.*, 1991; Dlugokencky *et al.*, 1998]. The emission increases from 515 Tg/yr in 1980 to 573 Tg/yr in 1996. In Table 1 we summarize our calculated yearly trends for the time period 1980 to 1996 in the OH distribution, in τ_{CH4}, and in the estimated global methane emission. The yearly average increase in methane emission is calculated from the observed changes in methane concentrations and the calculated changes in the τ_{CH4}. Included in the table are the estimated changes in OH and τ_{CH4} from Krol *et al.* [1998], and the estimated increase in methane emissions from Dlugokencky *et al.* [1998]; the latter is based on observed methane concentrations, and on a constant methane lifetime. The calculated change in methane lifetime, which is similar to the change calculated by Krol *et al.* [1998], implies a significant larger increase in emission than what is obtained from the observed methane changes assuming a constant methane lifetime [Dlugokencky *et al.*, 1998].

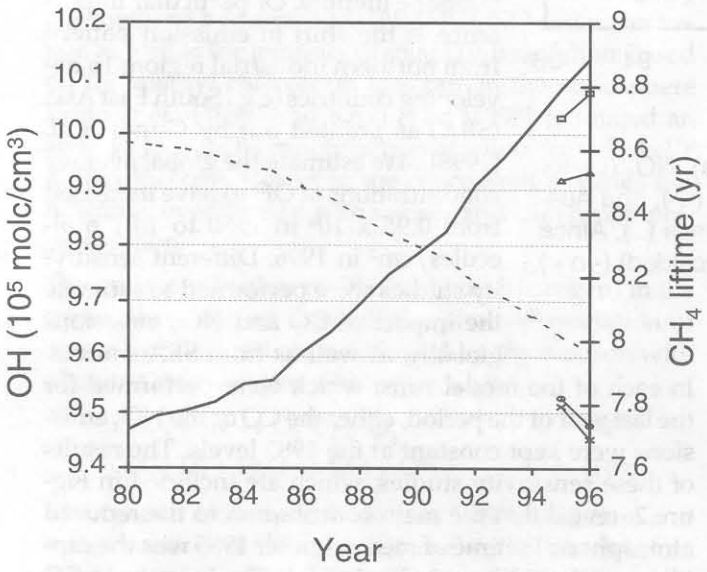

Figure 2. The change in global average OH concentration (—), and τ_{CH4} (- -) from 1980 to 1996 due to changes in emissions of CO, NOx, and NMHCs, and observed changes in CH_4. Calculations of τ_{CH4}; with the global NO_x emissions held at 1985 level (❑), with the South East Asia (Japan included) NO_x emissions held at the 1985 level (Δ), with the global CO emissions held at the 1985 level (x), with the South East Asia (Japan included) CO emissions held at the 1985 level (o).

Table 2. The ratio of CO to NO_x in the plumes from different biomass burning sources, and the change in methane lifetime with increasing emission from biomass burning. The impact from fossil fuel is for the global average increase between 1980 and 1996. $\Delta\tau_{CH4}$ is 8.34 years when all sources are included.

	CO/NO_x	$\Delta\tau_{CH4}$ (%)	$\Delta\tau_{CH4}/\Delta P_{NOX}$ (%/Tg(N))
Forest fire	103	0.8	0.6
Waste	93	1.7	0.8
Savannah burning	62	–0.4	–0.2
Biofuel	115	1.8	1.2
All biomass	88	3.2	0.4
Fossil fuel	20	–8.0	–1.4

The sensitivity of OH and methane lifetime to observed changes in stratospheric ozone (total ozone column) during the 1980s and 1990s was also studied, and a value for $(\Delta\tau_{CH4}/\tau_{CH4})/(\Delta TotO_3/TotO_3)$ in the range 0.28 to 0.76 was obtained. The value depends on latitude where and season when the depletion occurred. Average ozone depletion during the period 1988 to 1992 is calculated to have led to an additional reduction in the methane lifetime of 0.13% per yr.

It is of interest to estimate what increase in methane concentrations we would expect from the calculated increase in global methane emission if methane's lifetime were affected only by the increasing emission of methane through reaction R1 (no changes in the emissions of CO, NO_x and NMHC). In this case the mixing ratio of methane would be raised to 1.86 ppm in 1986 from a value of 1.57 in 1980 as compared to the observed value in 1996 of 1.76 ppm. This clearly demonstrate how important the emissions of precursors like NO_x and CO (particularly due to the rapid increase in fossil fuel SEA) are for the methane lifetime.

Observations have shown that there have been large variations in the atmospheric abundance in CO during the late 1980s and early 1990s (Novelli *et al.*, 1998). Part of the observed reductions can probably be explained by the decrease in fossil fuel related CO emissions given in Figure 1. However the large variation in emission from biomass burning over the time period studied has probably also contributed to the large CO variations. In order to study the impact of the changing emissions from biomass burning we have made several model runs with the 3-D Oslo CTM where the individual global biomass sources (forest fire, savannah burning, waste, biofuel) are removed one at a time [Isaksen *et al.*, 2000]. The resulting impact on [OH] and on τ_{CH4} is given in Table 2.

The large CO/NO_x ratio in most of the biomass burning emissions leads to a decrease in OH levels when the emission increases (reaction R4 dominates over reaction R6, except for savannah burning which has a smaller ratio) and leads to an increase in τ_{CH4}. This is in striking contrast to the impact of fossil fuel emission where enhanced emission leads to enhanced OH and reduced τ_{CH4}. This is due to a much smaller CO/NO_x ratio in fossil fuel emissions. In the situations with general increase in fossil fuel use the OH chemistry is dominated by reaction R6. The overall effect of biomass burning, even with the large observed variation in the emissions, has been much less than the effect of increasing fossil fuel use over the time period 1980 to 1996.

Carbon monoxide inter-annual variations and trends in the Northern Hemisphere: Role of OH.

Contributed by **Leonid Yurganov** (leonid@atmosp.physics.utoronto.ca), *Physics Department, University of Toronto, Canada.*

Introduction

Carbon monoxide (CO) is produced as a by-product of incomplete combustion of carbon-containing materials as well as due to photochemical conversion of atmospheric methane and other hydrocarbons. The main sources of CO are located at continental surfaces; the most important of them are human-related emissions (year-round) and biomass burning (dry seasons in tropics and warm part of the year in boreal areas). Photochemical conversion of hydrocarbons, e.g., methane, is an important source of CO, especially in summertime and the tropics. Reaction with hydroxyl radical is widely considered as the most significant sink for carbon monoxide (contributions of continental soil and ocean are very small for the CO global budget). At the same time, CO is usually the dominant reactant for OH, although other species in polluted or forested areas can be important [Brune, this issue; Wang, this issue]. As a result, OH distributions and trends should influence CO concentration dramatically. Dependence of OH concentration on the CO field is considerable as well. However, a detailed understanding of these relationships is not clear yet. The aim of this article is to consider available data on long-term variability of CO in relation to OH trends.

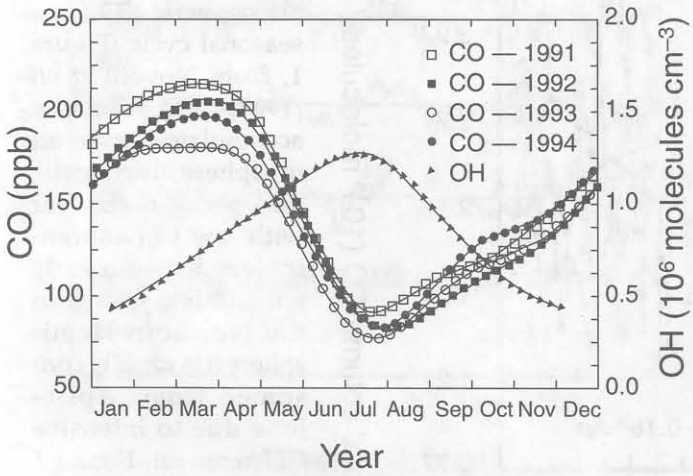

Figure 1. Overlay of smoothed CO and OH in the Northern Hemisphere. Biweekly CO mixing ratios were obtained by averaging CMDL network data. Biweekly OH concentrations were obtained from monthly concentrations provided by Spivakovsky *et al.* [1990]. Adapted from Novelli *et al.* [1998].

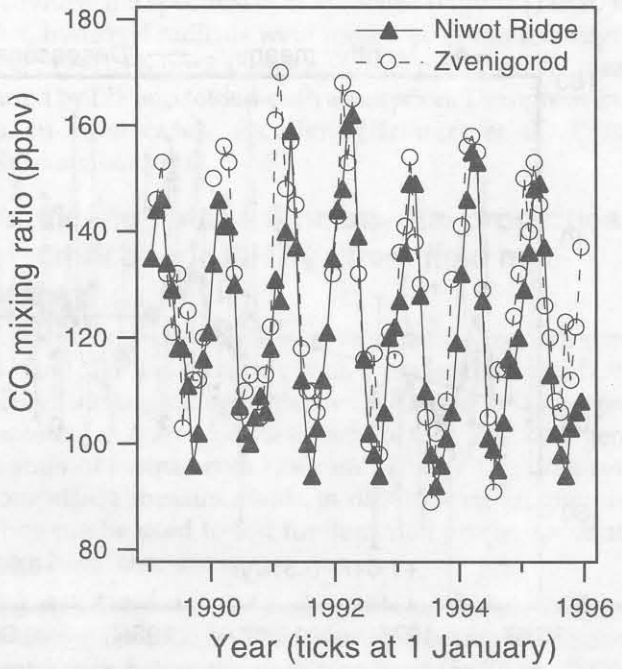

Figure 2. Tropospheric mean mixing ratio over Zvenigorod, Russia, compared to free tropospheric mixing ratio, sampled by CMDL/NOAA at the altitude of 3475 m above sea level at Niwot Ridge, Colorado, US.

Reference lists are available at http://web.mit.edu/igac/www

CO was discovered in the atmosphere through its absorption at the fundamental band near 4.6 μm [Migeotte, 1949] measured in the solar spectrum in late 1940s in the US and again at the International Scientific Station, Jungfraujoch, Switzerland. Systematic recording of CO bands in solar spectra started in Russia in 1970, at Kitt Peak Observatory in the US in 1976, and at the Jungfraujoch station in 1984. *In situ* measurements of this trace gas were made possible with the advent of the hot mercuric oxide technique [Robbins *et al.*, 1968; Seiler, 1974] and gas chromatography (GC) [Khalil and Rasmussen, 1994; Novelli *et al.*, 1998].

Table 1. A review of available estimates for CO trend in % per year. Arial is for spectroscopic measurements in the total column above the site (H is the height above sea level) or columns in some layers in the atmosphere (see the Layer column). *Italic* is for sampling in the surface layer (which is assumed to represent the marine boundary layer). Trend for Jungfraujoch, 1984–1997 according to WMO [1999].

Site and reference	H, km	Period	Trend, %/yr	STD, %/yr	Layer, km
Zvenigorod, Russia, this paper	0.2	1970-1982	+1.3	0.8	0.2-10
		1980-1995	+0.2	0.2	
		1984-1995	+0.4	0.2	
		1984-1997	+0.02	0.18	
Jungfrau., Switzer. (Mahieu *et al.*1995)	3.58	1950-1987	+0.85	0.08	Above 3.5
		1984-1995	-0.18	0.16	
		1984-1997	-0.53	0.18	
Kitt Peak, US (Rinsland *et al.*, 1988)	2.09	1978-1997	-0.27	0.17	2.1-14
NH, 20 sites (Novelli et al. 1998)	*0-0.2*	*1990-1995*	*-2.0*	*0.2*	*MBL*
NH, 2 sites (Khalil & Rasm. 1995)	*0-0.2*	*1981-1986*	*+0.8*	*0.7*	*MBL*
		1987-1992	*-1.4*	*0.9*	

It should be noted that solar spectroscopy and gas sampling techniques monitor CO in different atmospheric domains, namely, in the entire tropospheric layer above the site and in the surface layer, respectively. Moreover, most GC monitoring is conducted at remote islands or at coastal stations so as to minimize continental influence (e.g., NOAA / CMDL network); therefore the data mainly characterize the boundary layer over oceans. Only a few mountain observatories sample free tropospheric air over continents (e.g., Niwot Ridge, Colorado). An advantage of the solar spectroscopic method is an opportunity to apply new retrieval algorithms and updated line parameters to spectra measured in the past (e.g., re-analysis of Migeotte's spectra of early 1950s by Zander *et al.*, [1989]). In contrast, various *in situ* techniques require reference calibration mixtures and accuracy strongly depends on the consistency and validity of calibration procedures. A re-analysis of former results is usually questionable.

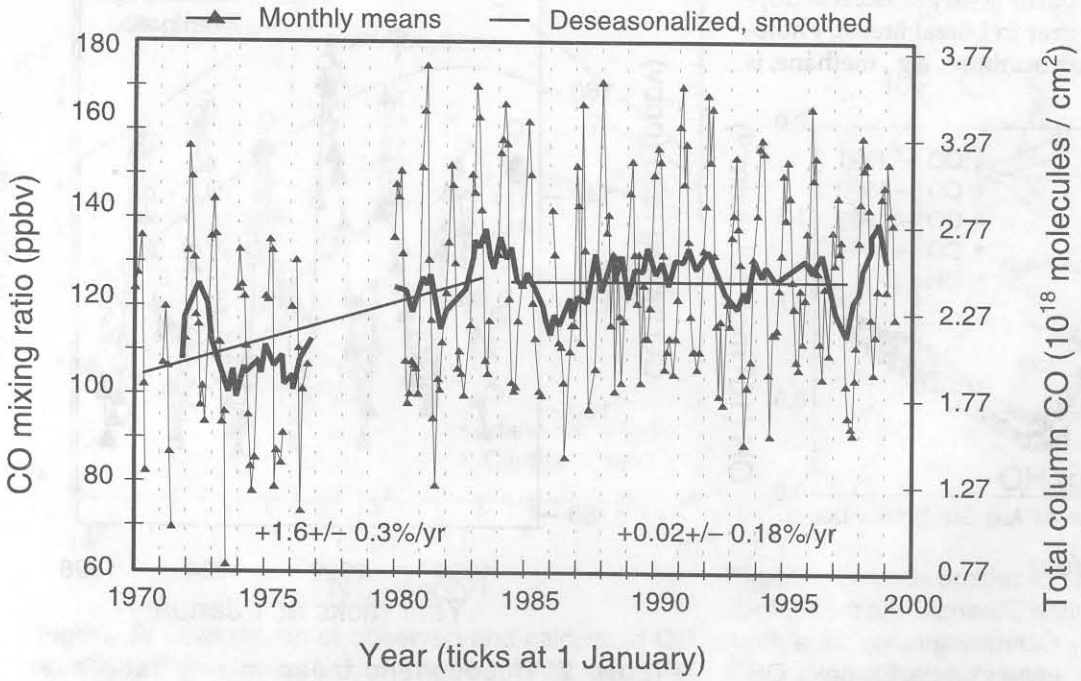

Figure 3. Total column CO abundance over Zvenigorod (right scale) and corresponding mean tropospheric mixing ratio (left scale). Regression lines for 1970-1984 and for 1985-1997 are shown.

An important feature of atmospheric CO is its seasonal cycle (Figure 1, from Novelli *et al.* [1998]). CO gradually accumulates in the atmosphere during the dark period of the year with low OH concentrations between early fall and late spring. In the Northern Hemisphere it is rapidly consumed from April–June due to intensive OH removal. Figure 1 illustrates a strong seasonal dependence of CO concentration on [OH]; interannual [OH] variations also should influence CO. A decline

of CO after the Pinatubo eruption is also visible in Figure 2, which shows mean monthly values for the layer 0-10 km in Zvenigorod plotted together with concurrent monthly mean local mixing ratios at 3.7 km altitude asl at the Niwot Ridge station in Colorado, US.

CO trend before and after the mid-1980s.

Both total column and *in situ* methods provided evidence in support of a positive CO trend between the 1950s and mid-1980s (Table 1). First, measurements of CO total column in Russia revealed a 1.3 % per year increase in January–October means between 1970 and 1982 [Dvoryashina et al., 1984; Dianov-Klokov and Yurganov, 1989] (see Figure 3). Spectra measured sporadically by M. Migeotte at the Jungfraujoch station in 1950-1951 were re-analyzed by Zander *et al.* [1989] and compared to similar measurements of 1985-1987. A positive trend of 0.85% per year was found. Khalil and Rasmussen [1994] derived a 0.8 % per year trend between 1981 and 1986. Analysis of air bubbles incorporated in Greenland glaciers revealed a 0.35 ppb per year (0.3 % per year) increase between 1850 and 1950 [Haan *et al.*, 1996].

However, estimates for CO trends after 1985 changed dramatically. A global CO decline of –2.6% per year in the boundary layer was observed by Khalil and Rasmussen [1994] between 1987 and 1992. Even higher rates of global decline (–5.6%/yr) were reported by Novelli *et al.* [1994] for the boundary layer during a relatively short period of 1991–1993 (explained mostly by a perturbation from the Pinatubo eruption, see below).

Total column CO also ceased to grow. Practically stable CO (-0.08 ± 0.5 %/yr) was found over Russia between 1983 and 1993 [Yurganov *et al.*, 1995]. Generally stable CO with irregular fluctuations was observed there after 1993 as well (see Figure 2). Total column CO in New Zealand also had no significant trend [0.37 ± 0.57%/yr, 1993-1997, Rinsland *et al.*, 1998]. Small negative trends were observed at Switzerland [–0.18 ± 0.16%/yr, 1984 - 1995, Mahieu *et al.*, 1997] and the US (–0.27 ± 0.17%/yr, 1978 -1997, Rinsland *et al.*, 1998].

One can conclude that stabilization or decrease of global CO concentration after mid-1980s after a long period of growth seems to be a real phenomenon. The question is how large is this deceleration: 2-3%/yr (as found by GC in the boundary layer) or 1-1.5 %/yr (for the total column)?

Possible explanations for changing trend

Several attempts have been made to explain the observed CO deceleration. Yung *et al.* [1999] concluded that a significant part of CO (and CH_4) change in trend can be explained by a change in biomass burning. Changes in anthropogenic CO production and UV increase due to the thinning of the ozone layer were considered by Novelli *et al.* [1994] and Mahieu *et al.* [1997] as possible explanations of the phenomenon.

This paper focuses on a [CO]-[OH] relationship. [OH] depends on UV radiation, determined by atmospheric attenuation by ozone and aerosols (see other papers in this issue). Yurganov *et al.* [1999] found that CO correlates both to stratospheric aerosol optical depth (AOD)

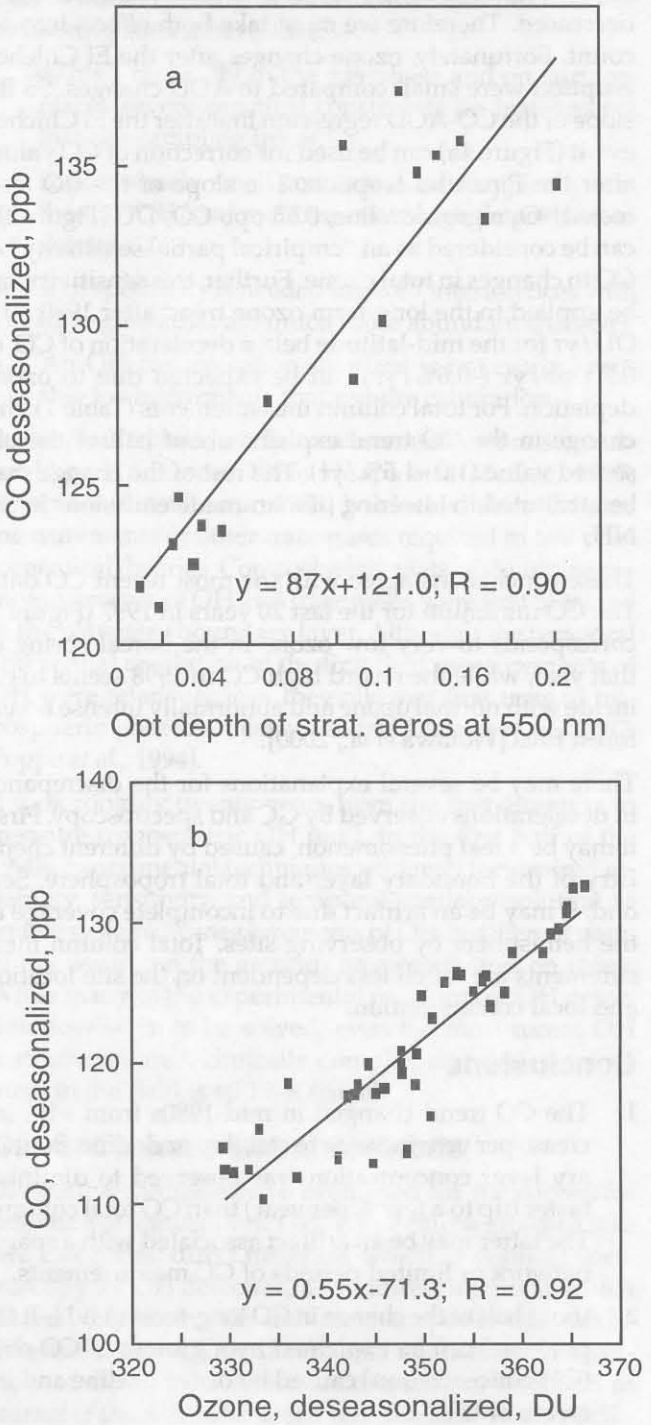

Figure 4. a) Correlation between CO and aerosol optical depth (AOD) at 550 nm for 17 months after the El Chichon eruption. b) Correlation between monthly mean CO, reduced to AOD=0, using the slope from Figure 4a, and total ozone for 38 months just after the Pinatubo eruption.

Reference lists are available at http://web.mit.edu/igac/www

and to total ozone after major eruptions. There were two volcanic eruptions since the early 1980s that significantly perturbed stratospheric aerosol on a global scale: El Chichon in April 1982 and Mt. Pinatubo in June 1991. The problem is that both aerosol and ozone are changed after major eruptions; aerosol is increased and ozone is decreased. Therefore we must take both effects into account. Fortunately, ozone changes after the El Chichon eruption were small compared to AOD changes. So the slope of the CO-AOD regression line after the El Chichon event (Figure 4a) can be used for correction of CO values after the Pinatubo eruption. The slope of the CO (corrected)–O_3 regression line, 0.55 ppb CO/DU (Figure 4b) can be considered as an "empirical partial sensitivity" of CO to changes in total ozone. Further, this sensitivity can be applied to the long-term ozone trend after 1980: –1.3 DU/yr for the mid-latitude belt; a deceleration of CO of 0.7 ppb/yr (-0.6%/yr) can be expected due to ozone depletion. For total column measurements (Table 1), this change in the CO trend explains about half of the observed value (1.0 –1.5%/yr). The rest of the change may be attributed to lowering of man-made emissions in the NH.

These conclusions agree with the most recent CO data. The CO minimum for the last 20 years in 1997 (Figure 1) corresponds to very low ozone in the boreal spring of that year, while the record high CO in 1998 seems to coincide with normal ozone and abnormally intense boreal forest fires [Wotawa *et al.*, 2000].

There may be several explanations for the discrepancy in decelerations observed by GC and spectroscopy. First, it may be a real phenomenon, caused by different chemistry of the boundary layer and total troposphere. Second, it may be an artifact due to incomplete coverage of the hemisphere by observing sites. Total column measurements are much less dependent on the site location and local contamination.

Conclusions

1. The CO trend changed in mid-1980s from ~1% increase per year increase to stability or decline. Boundary layer concentration was observed to diminish faster (up to a few % per year) than CO total column. The latter may be an artifact associated with a sparse network or limited periods of GC measurements.
2. About half of the change in CO long-term trend (~0.6% per year) can be explained by a growth of CO sink (OH concentration) caused by ozone decline and increase of UV.
3. The rest of the change in CO trend may be attributed to a change in CO sources (human-induced emissions, biomass burning or photochemical conversion of hydrocarbons).

Global tropospheric OH: Observational constraints and model simulations

Contributed by **Yuhang Wang** (yhw@envsci.rutgers.edu), *Rutgers University, USA.*

The abundance of tropospheric hydroxyl radicals (OH) largely defines the oxidizing capacity of the atmosphere. A healthy level of tropospheric OH keeps in check atmospheric concentrations of many potent greenhouse gases such as CH_4 and HCFCs and prevents large amounts of O_3-depleting halogenated hydrocarbons from reaching the stratosphere. Monitoring global tropospheric OH concentrations and understanding the controlling factors, both anthropogenic and natural, are necessary to protect our living environment. I will briefly review recent scientific works related to these two global issues.

Introduction

A tutorial of simplified OH chemistry is in order. In the troposphere, OH production is largely initiated by photolysis of O_3 to $O(^1D)$, O atoms in an energetically excited state, which reacts with H_2O,

$$O_3 + h\nu \rightarrow O(^1D) + O_2 \qquad (R1)$$

$$O(^1D) + H_2O \rightarrow 2OH \qquad (R2)$$

The reaction sequence leads to primary production of OH since an OH radical (with an unpaired electron) is produced from a much more stable molecule. A large fraction of OH is recycled during oxidation of reduced compounds in the presence of nitrogen oxides (NO_X = NO + NO_2),

$$OH + CO + (O_2) \rightarrow HO_2 + CO_2 \qquad (R3)$$

$$HO_2 + NO \rightarrow OH + NO_2 \qquad (R4)$$

$$NO_2 + h\nu + (O_2) \rightarrow NO + O_3 \qquad (R5)$$

In this sequence, a CO molecule is oxidized to CO_2 and an O_3 molecule is produced. Radicals of HO_X ($OH+HO_2$) and NO_X are conserved. Removal of OH is generally through the self reaction of its HO_X-family sibling, HO_2,

$$HO_2 + HO_2 \rightarrow H_2O_2 + O_2 \qquad (R6)$$

H_2O_2 is lost from the atmosphere by deposition to surface and rainout.

Although highly simplified (see Brune, this issue, for more detail), the above scheme suggests that in order to understand tropospheric OH, it is necessary that we understand the distributions of O_3, NO_X, CO (and hydrocarbons), water vapor, solar radiance (for photolysis), and atmospheric deposition processes. Global simulations of OH, its precursors, and its proxies are generally

carried out using 3-D models. In the following section, I will describe atmospheric observations that can be used to constrain tropospheric OH concentrations. In the discussion on global OH modeling, I will examine three categories, constrained respectively by emission sources and atmospheric transport, observed distributions of OH precursors, and observed distributions of OH proxies. The division among the categories is somewhat artificial but streamlines the discussion.

Constraints from observations

Dorn and Hofzumahaus [this issue] review instruments employed for *in situ* measurement of OH near the surface or onboard aircraft, and the comparison studies among these observations and model simulations. Surface observations are occasionally lower than model results at continental sites; heterogeneous loss of HO_2 to surfaces or unknown biogenic hydrocarbons, not measured at the sites, may account for the difference [e.g., McKeen *et al.*, 1997]. Jaeglé [2000] reviewed upper tropospheric OH measurements in comparison to model simulations for recent aircraft campaigns; measurements generally support the current understanding of HO_X chemistry. The issues of additional HO_X sources not from reactions R1-2 are also discussed by Brune [this issue]. Although significant for OH concentrations in the upper troposphere, these issues bear far less significance on model predictions of the global mean OH concentration, which are largely dictated by concentrations in the lower and middle tropical troposphere [Spivakovsky *et al.*, 2000]. The most comprehensive *in situ* measurements of regional OH concentrations to date were conducted onboard DC-8 and P-3 aircraft over the tropical Pacific during the Pacific Exploratory Mission (PEM)-Tropics B. Good agreement was found between observed and simulated OH concentrations [Tan *et al.*, 2000; Mauldin *et al.*, 2000], lending some confidence to model simulations of tropospheric OH.

Direct monitoring of tropospheric OH on a global scale is unattainable at present. The global mean OH concentration, however, can be estimated indirectly from the concentrations of proxy gases, such as CH_3CCl_3 [Singh, 1977; Lovelock, 1977], through budget calculations. Good proxy gases have known source distributions, relatively long atmospheric lifetimes, significant OH oxidation compared to other loss pathways, and long-term measurements. Spivakovsky *et al.* [2000] reviewed five commonly used proxies, CH_3CCl_3, HCFC-22, CH_2Cl_2, C_2Cl_4, and ^{14}CO. Observations of ^{14}CO turned out to be most difficult to interpret. The lifetime of ^{14}CO against OH oxidation is 1-2 months in the tropics and midlatitude summer. The short lifetime implies high sensitivities of observed concentrations to transport of cosmically generated ^{14}CO in the stratosphere and high latitudes to the lower-latitude troposphere. The lifetimes of CH_2Cl_2 and C_2Cl_4 are also short in the tropics, 2 and 4 months, respectively. However, the industrial proxies have better known source strength and distribution. Particularly since their anthropogenic sources are mostly located at northern midlatitudes, the north-south gradients of their concentrations pose some constraints on the global and hemispheric means of OH concentrations. Observations of CH_2Cl_2 are more useful because of Cl-oxidation of C_2Cl_4. In comparison, CH_3CCl_3 has a lifetime of about 5 years accompanied by decade-long observations around the globe, making it an ideal proxy for global tropospheric OH [e.g., Prinn *et al.*, 1995]. The atmospheric lifetime of HCFC-22 is about 11 years [Miller *et al.*, 1998]. As the concentrations continue to grow in the atmosphere, the constraints afforded by HCFC-22 observations will be increasingly important. The proxy constraints, although powerful, depend on the accuracy of source magnitudes and distribution, absolute measurement calibration, loss pathways other than OH oxidation, and kinetic data for the reaction with OH. The cumulative uncertainty in derived global mean OH concentration is up to 20-30% [Spivakovsky *et al.*, 2000].

Chemistry and transport modeling

This class of modeling, unlike the other two discussed in following sections, is not specifically designed to simulate tropospheric OH. It simulates the primary components of the natural system, emissions, atmospheric transport, chemistry, and deposition. As reactions R1-6 implied, tropospheric O_3-HO_X-NO_X-CO-hydrocarbon chemistry is tightly coupled. Emissions for NO_X, CO and nonmethane hydrocarbons (NMHCs) in the models include anthropogenic sources from fossil fuel combustion, industry, and biomass burning, and natural sources from vegetation (isoprene, terpenes, acetone), lightning (NO_X), and soils (NO_X). Concentrations of CH_4, well mixed in the troposphere, are generally specified in the models. The uncertainties in emission estimates, except for fossil fuel combustion and industry, are a factor of 2 or more. Transport is generally simulated in the models using meteorological fields from a general circulation model or weather forecast model. Extensive model evaluations for all related species using observations from surface sites, balloons, aircraft, and satellites, are carried out to ensure the quality of model results [e.g., Müller and Brasseur, 1995; Roelofs and Lelieveld, 1995; Berntsen and Isaksen, 1997; Wang *et al.*, 1998a; Hauglustaine, 1998; Lawrence *et al.*, 1999]. The complexity of the models offers the flexibility to investigate various factors affecting the system, including sources of NO_X [Larmarque *et al.*, 1996; Penner *et al.*, 1998; Horowitz and Jacob, 1999; Levy *et al.*, 1999], CO [Holloway *et al.*, 2000], and NMHCs [Houweling *et al.*, 1998; Wang *et al.*, 1998b; Poisson *et al.*, 2000], emissions from aircraft [e.g. Brasseur *et al.*, 1996] and ships [Lawrence and Crutzen, 1999; Kasibhatla *et al.*, 2000], O_3 transport from the stratosphere [Roelofs and Lelieveld, 1997; Wang *et al.* 1998b; Lelieveld and Dentener, 2000], and heterogeneous chemistry [e.g., Dentener and Crutzen, 1993; Lary *et al.*,1997].

Reference lists are available at http://web.mit.edu/igac/www

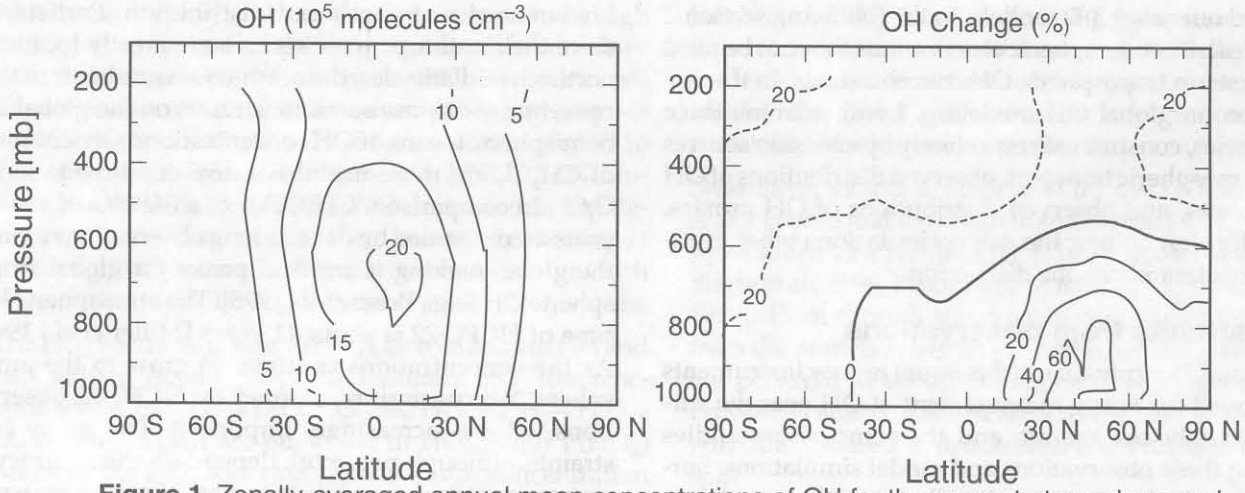

Figure 1. Zonally-averaged annual mean concentrations of OH for the present atmosphere and percentage changes from preindustrial times to present. Adopted from Wang and Jacob [1998].

One particularly relevant issue is the change of tropospheric composition since preindustrial times. Wang and Jacob [1998] reviewed available observations for preindustrial times and found the best constraints existed for near-surface O_3. Even these (reconstructed) records have seasonal and altitude variations that can hardly be reconciled with our current understanding of tropospheric O_3. They estimated that the sources of NO_X (S_N) and of CO and hydrocarbons (S_C) increased by factors of 4.7 and 2.5, respectively, from preindustrial times to present. Whereas both sources contribute, respectively by 60% and 40%, to the estimated 60% increase in the global O_3 burden, they have offsetting effects on the global mean OH concentration [Thompson, 1992]. Wang and Jacob [1998] showed a model sensitivity of

$$\Delta[OH] \propto \Delta(S_N / S_C^{3/2})$$

resulting in a 9% decrease of the global (mass-weighted) mean OH concentration from preindustrial times in their model. Their results of much smaller OH change compared to O_3 are consistent with other global 3-D model studies [e.g., Crutzen and Zimmermann, 1991; Martinerie *et al.*, 1995; Levy *et al.*, 1997; Roelofs *et al.*, 1997; Berntsen *et al.*, 1997; Mickley *et al.*, 2000]. Figure 1 shows the zonally-averaged annual mean OH concentrations for the present atmosphere and model simulated changes from preindustrial times. Large increases of 20-60% occur in the lower troposphere of the Northern Hemisphere while decreases of about 20% take place in the northern upper troposphere and most of the Southern Hemisphere. The asymmetry reflects the longer range transport of CO and hydrocarbons than that of NO_X. The distribution shift toward warmer lower troposphere from preindustrial times boosts OH oxidation of CH_3CCl_3, the rate of which increases with temperature; the model estimated the same 5.1 years for the lifetimes of tropospheric CH_3CCl_3 against OH oxidation for preindustrial times and present.

Precursor-constrained modeling

Uncertainties in emissions and atmospheric transport can be minimized to some extent by constraining the model using atmospheric observations. Spivakovsky [2000] carefully compiled climatologies for meteorological variables and OH precursors including O_3, CO, NO_X, and hydrocarbons from available atmospheric observations and applied them to global OH simulations. This work heralds the 3-D chemical data assimilations that will take the center stage in the years to come. Figure 2 shows the simulated annual mean OH distribution. The resulting lifetime of tropospheric CH_3CCl_3 against OH oxidation is 4.8 years. The striking difference compared to Figure 1 is the symmetry in OH distribution across the Equator. The two results have about the same mean OH concentrations in the Northern Hemisphere but Figure 2 is higher by 30% in the Southern Hemisphere. The interhemespheric asymmetry with higher OH concentrations in the Northern Hemisphere, as illustrated in Figure 1, is common among chemistry and transport models. The more up-to-date simulation by Mickley *et al.* [2000] shows mean OH concentrations 16% higher in the Northern than Southern Hemisphere. The smaller interhemispheric ratio is due solely to less OH in the Northern Hemisphere compared to Wang *et al.* [1998a].

The interhemispheric OH asymmetry in chemistry and transport models arises from the asymmetry in anthropogenic emissions, which boost OH in the vicinity but depress OH in remote areas (Figure 1). The latter effect was observed over the tropical Pacific during PEM-Tropics B [Wang *et al.*, 2000]. Presently most models have symmetric (across equator) biomass burning emissions, the only large anthropogenic source in the Southern Hemisphere. A symmetric OH distribution would imply much larger emissions from biomass burning in the southern than northern tropics.

The observational evidence for a hemisphere-symmetrical OH distribution is not yet affirmative. Observations of CH_3CCl_3 tend to support this distribution [Spivakovsky *et al.*, 2000; Montzka *et al.*, 2000]. The constraint on the inter-hemispheric ratio will improve to ±50% as CH_3CCl_3 emissions are phased out [Spivakovsky *et al.*, 2000]. Montzka *et al.* [2000] suggested that the air mass boundary is more appropriately defined by the Inter-Tropical Convergence Zone (ITCZ), the annual-mean position of which is north of the equator. They found that CH_3CCl_3 observations implied a higher mean OH concentration in the southern than northern air mass. The observations of ^{14}CO also support the symmetric distribution or even a higher mean OH concentration in the Southern Hemisphere [e.g., Brenninkmeijer *et al.*, 1992]; however, the interpretation is marred by large uncertainties in ^{14}CO transport [Spivakovsky *et al.*, 2000; Quay *et al.*, 2000]. Observations of CH_2Cl_2 suggest, on the other hand, higher OH concentrations by 45-95% in the northern than Southern Hemisphere [Spivakovsky *et al.*, 2000].

Proxy-gas constrained modeling

This class of modeling takes full advantage of long-term observations of OH proxy gases using sophisticated statistical analysis. The best data series to date was gathered by the Atmospheric Lifetime Experiment / Global Atmospheric Gas Experiment (ALE / GAGE). Prinn *et al.* [1995] and Krol *et al.* [1998] applied different statistical methods to analyze the data series from 1978 to 1993. Global HCFC-22 measurements have been collected since 1992 by the NOAA Climate Monitoring & Diagnostics Laboratory (CMDL); the program also measures CH_3CCl_3 (beginning in 1988). Miller *et al.* [1998] demonstrated the utility of HCFC-22 observations using the method similar to Prinn *et al.* [1995] and found results consistent with the earlier work.

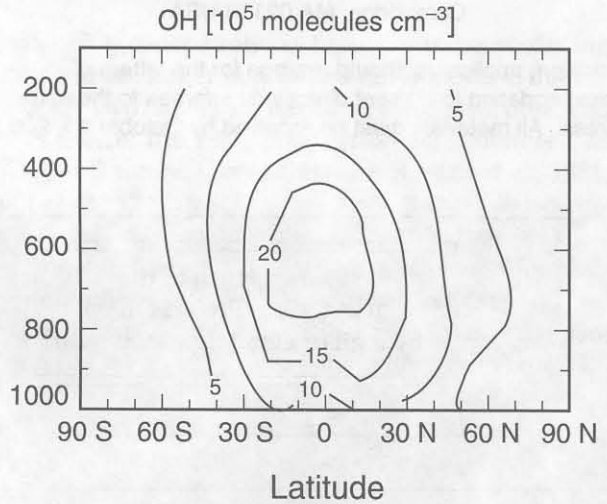

Figure 2. Zonally-averaged annual mean concentrations of OH for the present atmosphere computed by Spivakovsky *et al.* [2000]. (Courtesy of C.M. Spivakovsky.)

The gist of the modeling technique is trying to deduce global OH concentrations from proxy observations; I will discuss the case for CH_3CCl_3. The deduction is an inverse problem since the observed atmospheric accumulation of CH_3CCl_3 results from industrial emissions, OH oxidation, and minor losses to the oceans and in the stratosphere. Starting with *a priori* global OH distribution, the inverse modeling aims to find the global mean OH concentration and its linear trend (with respect to time) that best fit observed CH_3CCl_3. A long-term data series is essential for the inversion. The *a priori* global OH distribution is taken from a global chemistry and transport model like the ones previously discussed. Prinn *et al.* [1995] used a 2-D model and Krol *et al.* [1998] relied on the 3-D model by Crutzen and Zimmermann [1991]. Prinn *et al.* [1995] applied a recursive weighted least squares (Kalman) filter to the inversion. With a more complicated 3-D OH distribution, Krol *et al.* [1998] employed a Monte-Carlo ensemble method for the fitting optimization.

Prinn *et al.* [1995] derived an atmospheric lifetime of CH_3CCl_3 of 4.6 years with no apparent trend from 1978-1994. Krol *et al.* [1998] found a similar CH_3CCl_3 lifetime of 4.5-4.7 years but an increasing trend of 7% in 15 years. The estimated global mean (mass-weighted) OH concentration from the two studies is 9.7-10.7x10^5 molecules cm^{-3} in the troposphere. Prinn and Huang [2000] and Krol *et al.* [2000] examined the causes for the trend discrepancy. The different treatment of CH_3CCl_3 concentrations at the beginning of the observation series appears to be a significant factor. Prinn *et al.* [1995] computed CH_3CCl_3 concentrations from 1951 and had only two free parameters (mean OH and trend) in their inverse model. Krol *et al.* [1998], on the other hand, computed CH_3CCl_3 concentrations from 1978 and needed a third optimizing parameter to adjust model initial CH_3CCl_3 concentrations.

The 7% OH increase from 1978 to 1993 estimated by Krol *et al.* [1997] is significant in light of ±10% change from preindustrial times to present found in most global 3-D simulations [Wang and Jacob, 1998]. One factor not considered in the other global 3-D studies is the decrease of stratospheric O_3 concentrations since the late 1970s, which, Krol *et al.* [1998] estimated, contributes to a 2% increase of the global mean OH concentration. They suggested that increasing water vapor concentrations in the tropics and a decoupling of NO_x and CO emissions (with increasing NO_x but decreasing CO emissions) by about 10% each could explain the rest of the OH increase. A shift in the global mean OH concentration by this magnitude would therefore signify substantial changes taking place in anthropogenic emissions or global climate. Resolving the difference between the two studies and obtaining additional independent estimates are critical.

Acknowledgements

I thank Clarissa Spivakovsky and Loretta Mickley for informative discussion and data.

Reference lists are available at http://web.mit.edu/igac/www

Announcements

Challenges of a Changing Earth

A Global Change Open Science Conference
Amsterdam, The Netherlands
10-13 July 2001

International Geosphere-Biosphere Programme (IGBP)
International Human Dimensions Programme on Global Environmental Change (IHDP)
World Climate Research Programme (WCRP)

Phone: +46-8-16-64-48; Fax: +46-8-16-64-05
http://www.sciconf.igbp.kva.se/

For further information, contact:
Rowena Foster (Rowena.Foster@dwe.csiro.au)

Rationale and Philosophy

From its inception the IGBP has worked towards an overall goal: to describe and understand the interactive physical, chemical and biological processes that regulate the Earth system, the unique environment it provides for life, the changes that are occurring, and how they are influenced by human actions. IGBP and its Core Projects have now been in the implementation phase for a decade, and the time is now right for a first IGBP-wide open science conference to highlight not only the increasingly integrated research across the IGBP community, but also the growing links to WCRP and IHDP.

The Global Change Open Science Conference will present the latest scientific understanding of global environmental change at three levels: (i) the integrated level of the IGBP core projects and the IGBP as a whole; (ii) cross-cutting research involving the WCRP and IHDP, as well as regional research coordinated by START and other groups; and (iii) the individual level of the research projects which contribute to IGBP/WCRP/IHDP networks and provide the broad, substantive base on which the integrating activities of the three programmes are built.

The Conference will also look forward. The last day will present the visionary and creative new approaches in Earth System Science, for studying the thresholds, nonlinearities and teleconnections of a complex planetary system in which human activities are intimately interwoven with natural processes. It will outline a research programme for our current era of increasing human domination of many global-scale processes - the "Anthropocene".

Molina Fellowship in Environmental Science

The Molina Fellowship in Environmental Science was established to bring postdoctoral fellows and young scientists from emerging nations to MIT to pursue studies in environmental sciences. Molina Fellows will then return to their home countries better able to address complex environmental concerns. Individuals holding a Ph.D. degree in science or engineering and interested in pursuing work in environmental science are eligible for the one-year Fellowship with an annual stipend of $35,000.

Qualified scientists are encouraged to apply by sending a Curriculum Vitae with a list of publications, names and addresses of three professional references and a brief statement of research interest to the attention of:

Professor Ronald G. Prinn, Head
Earth, Atmospheric and Planetary Sciences
Massachusetts Institute of Technology, Bldg 54–918
77 Massachusetts Avenue
Cambridge, MA 02139 USA

In addition, applicants should arrange for the letters of recommendation to be sent directly by referees to the same address. All materials must be received by October 15, 2000.

Please help us keep our mailing list up to date:

_____ Please note my new address
_____ Please also send IGAC*tivities* to my colleague
_____ Please remove me from your mailing list

Please return to the IGAC Core Project Office by mail or email (igac@mit.edu)

Name: _____ Organization: _____

Street address: _____

City: _____ State: _____ Zip: _____ Country: _____

Telephone: _____ Fax: _____ E-mail: _____

IGAC Symposium:
Atmospheric Chemistry in the Tropics:
From Local to Global,
From Air Pollution to Climate Change

Institute of Environmental Research
Chulalongkorn University
Bangkok, Thailand
23-23 January 2001

Tel. (66 2) 218-8126 to 9; Fax. (66 2) 255-4967
http://www.start.or.th/IGAC7/

For information, contact:
Professor Jariya Boonjawat (jariya@start.or.th)

NARSTO Technical Conference on Aerosol Science
Querétaro, Mexico
October 24-26, 2000
http://www.cgenv.com/Narsto/mex1.html

AAAR 2000 – 19th Annual Conference
American Association for Aerosol Research (AAAR)
St. Louis, Missouri, USA
November 6-10, 2000
Phone: (+1)(513)742-2227; Fax: (+1)(513)742-3355
Further information: mail@aaar.org
http://www.aaar.org/00annmtg.htm

7th International Conference on Carbonaceous
Particles in the Atmosphere
University of Puerto Rico
November 26-29, 2000
Phone: (+1)(787) 764-8369; Fax: (+1)(787) 756-7717
Further information: iccpa@adam.uprr.pr.
http://web.uprr.pr/iccpa/

The 6th Gordon Conference on Gaseous Ions
February 25 - March 2, 2001
Ventura Beach Hotel, Ventura California
Phone (+1)(401) 783-4011
Fax(+1)(401) 783-7644
http://www.chem.utah.edu/ion-grc/

European Research Course on Atmospheres 2001
Centre National de la Recherche Scientifique
Universite Joseph Fourier
Grenoble, France
9 January – 9 February 2001
+33 4 76 82 42 62; Fax: +33 4 76 82 42 01
Further information: :michele@glaciog.ujf-grenoble.fr

A Changing Atmosphere
8th European Symposium on the Physico-Chemical
Bevahiour of Atmospheric Pollutants
European Commission; DG Research;
Joint Research Centre;
17-20 September 2001
Torino, Italy
Tel +39 0332 789958; Fax +39 0332 785704
Further information: frank.raes@jrc.it
http://www.ei.jrc.it/ap/events/torino2001/

Climate Conference 2001
Netherlands Centre for Climate Research (CCR) and
Utrecht University, The Netherlands
20-24 August 2001
Phone: (+31/0) 030 253 3275;
Fax: (+31/0) 030 254 3163
climateconference2001@fbu.uu.nl"
http://www.phys.uu.nl/~wwwimau/cc2001.html

IGAC *tivities* Newsletter

Editor, Alex Pszenny
Layout and proofreading, Ed Carlevale
IGAC logo, Linda Kubrick

Published by The IGAC Core Project Office, MIT,
Room 24-409, Cambridge, MA 02139-4307, USA

Tel: (+1-617) 253-9887, Fax: (+1-617) 253-9886
E-mail: igac@mit.edu; http://web.mit.edu/igac/www/

IGAC was initiated by the Commission on Atmospheric Chemistry and Global Pollution (CACGP) and is a Core Project of the International Geosphere-Biosphere Programme (IGBP). The IGAC Core Project Office is currently supported by the National Science Foundation (NSF), National Aeronautics and Space Administration, National Oceanic and Atmosphere Administration, and Department of Energy of the United States of America through NSF Grant No. ATM 96-32757. Any opinions, findings and conclusions, or recommendations expressed in this newsletter are those of the individual author(s) and do not necessarily reflect the views of the NSF or other agencies.